

Depth and Position Sensing for an Autonomous Underwater Vehicle

Elliot Alfirevich

Bachelor of Engineering
Final Year Project Thesis, 2005

Mobile Robotics Laboratory,
Centre for Intelligent Information Processing Systems,
School of Electrical, Electronic and Computer Engineering,
The University of Western Australia.



Supervisor

Associate Professor Thomas Bräunl

Letter of Transmittal

Elliot Alfirevich
15 The Broadwater
BALLAJURA, WA, 6066

31st October 2005

The Dean
Faculty of Engineering, Computing and Mathematics
The University of Western Australia
35 Stirling Highway
CRAWLEY, WA, 6009

Dear Professor Mark Bush,

I submit to you with pride this dissertation entitled *Depth and Position Sensing for an Autonomous Underwater Vehicle* in partial fulfilment of the requirements of the award of Bachelor of Engineering with Honours.

Yours faithfully,

Elliot Alfirevich

Abstract

This project is concerned with the design and development of sensors for UWA's Autonomous Underwater Vehicle (AUV), *Mako*.

Depth and Position Sensing for an Autonomous Underwater Vehicle details the integration of a new pressure sensor for instantaneous depth measurement, and the design of a sonar transducer multiplexing system for lateral distance measurement in multiple directions.

Through instantaneous depth measurement, the AUV *Mako* can be protected from damaging pressures at depths below the maximum ratings of its components. Instantaneous depth measurement, combined with a suitable control strategy such as PID or Fuzzy Logic, gives *Mako* closed-loop depth control – the ability to "hover" underwater.

With the addition of the sonar multiplexing system, obstacles and walls will be detected with the minimum possible latency by allowing the sampling of any two of the four sonar transducers simultaneously. The sonar multiplexing system is controlled by *Mako's* EyeBot controller and designed to limit the interference effects resulting from operating two acoustic sonar transducers simultaneously in the same body of water.

Acknowledgements

Working on this project with the *Centre For Intelligent Information Processing Systems* has been the largest and most fulfilling task I've had the opportunity to undertake in my university life. Firstly, I'd like to thank Associate Professor Thomas Bräunl. Without Thomas' kind help and guidance this project may not have progressed this point.

A special thanks goes to Chris Thorp and his family. Moving the AUV and getting it in the pool takes two people. Without Chris' help the pool sessions would not have been as memorable.

I'd like to thank the EE Workshop staff, particularly Jonathon Brant, Ivan Neubronner and Mark Henderson, for the time and effort they have contributed to this project. I'll remember most Mark's passing questions, "Did it sink?" and Jon's speedy effort when we realised there was a problem with the Sonar Multiplexing circuit.

I'd like to thank everyone who has assisted me in reaching the completion of this project and reaching this point in my tertiary education. My family, Barry, Elizabeth and Sheridan Alfirevich and my girlfriend, Tamara Erdash - their love and support has helped me through this year.

Exchange students Bernhard Gerl, Michael Drtil, Thorsten Ruehl and Kalle Ohlsson, and the final year students Evan Broadway, Aaron Cha, Phil Bastian and Yuma Iwasaki - thanks for your help and friendship. It has been an unforgettable year with many memorable hours spent in the Mobile Robot Lab and the Teaching Lab 3.09.

Table of Contents

LETTER OF TRANSMITTAL	I
ABSTRACT	III
ACKNOWLEDGEMENTS	V
TABLE OF CONTENTS	VII
NOMENCLATURE	XI
ABBREVIATIONS AND ACRONYMS.....	XI
NAUTICAL TERMINOLOGY AND DIRECTIONS.....	XII
LIST OF VARIABLES	XIII
LIST OF FIGURES	XV
CHAPTER 1 INTRODUCTION	1
1.1 REMOTELY OPERATED VEHICLES (ROVs).....	1
1.2 AUTONOMOUS UNDERWATER VEHICLES (AUVs)	2
1.3 PROJECT MAKO	2
1.4 PROJECT MOTIVATION	3
1.4.1 <i>The Depth Pressure Sensor</i>	4
1.4.2 <i>The Sonar Multiplexing System</i>	4
1.5 THESIS OUTLINE.....	5
CHAPTER 2 BACKGROUND THEORY AND TECHNOLOGIES	6
2.1 PRESSURE, FLUID PRESSURE AND DEPTH	6
2.1.1 <i>Units of Pressure</i>	6
2.1.2 <i>Hydrostatic Pressure and Pascal's Law</i>	7
2.1.3 <i>Boyle's Law</i>	7
2.1.4 <i>Pressure at Water Depth</i>	7
2.2 DEPTH PRESSURE TRANSDUCERS AND SENSORS	8
2.2.1 <i>Research AUVs</i>	8
2.2.1.1 Sensotec TJE-series Pressure Sensor.....	8
2.2.1.2 Global Water Instruments WL400 Transducer	9
2.2.1.3 Motorola MPX5100DP.....	9
2.2.2 <i>Commercial ROVs and AUVs</i>	10
2.2.2.1 Sea-bird SBE 50 Digital Oceanographic Pressure Sensor	10
2.3 SONAR AND DISTANCE MEASUREMENT	11
2.3.1 <i>Passive and Active Sonar</i>	11
2.3.2 <i>Principles of Active Sonar</i>	12
2.3.2.1 Speed, Distance and Time	12
2.3.2.2 Finite Power	15
2.3.2.3 Multipath Fading.....	15

<i>The Navman Depth 2100</i>	17
2.4 SERIAL DATA COMMUNICATION	17
2.4.1 <i>Serial Communication</i>	17
2.4.1.1 Electrical Connection.....	18
2.4.1.2 Start and Stop Bits & Baud Rate.....	18
2.4.1.3 Parity	19
2.4.1.4 Data Bits	19
2.4.1.5 Sender and Receiver Configuration	19
2.4.2 <i>The EyeBot Controller</i>	19
2.4.3 <i>The NMEA 0183 Protocol</i>	20
2.5 CONTROL THEORY	21
2.5.1 <i>Proportional or P-Control</i>	21
2.5.2 <i>Fuzzy Logic</i>	21
CHAPTER 3 DEPTH PRESSURE SENSOR DESIGN	23
3.1 IMPORTANCE OF DEPTH SENSING.....	23
3.2 DESIGN REQUIREMENTS AND AIMS	24
3.3 PRESSURE TRANSDUCER – SENSYM SX15GD2.....	25
3.3.1 <i>Specifications and Features</i>	25
3.3.2 <i>Electronic Characteristics</i>	26
3.3.2.1 Equivalent Circuit - Semiconductor Wheatstone Bridge.....	26
3.3.2.2 Temperature Characteristics.....	26
3.4 COMPENSATION AND AMPLIFICATION CIRCUIT	28
3.5 FABRICATION AND CALIBRATION	30
3.5.1 <i>Fabrication</i>	30
3.5.2 <i>Calibration</i>	31
3.6 MECHANICAL DESIGN.....	32
3.7 MOUNTING THE DEPTH PRESSURE SENSOR ON MAKO.....	33
CHAPTER 4 SONAR MULTIPLEXING SYSTEM DESIGN	35
4.1 IMPORTANCE OF SONAR.....	35
4.2 DESIGN REQUIREMENTS AND AIMS	35
4.3 CONTROLLER NMEA 0183 MULTIPLEXING.....	37
4.3.1 <i>PICAXE-18X Microcontroller</i>	38
4.3.2 <i>TTL/CMOS and RS-232</i>	38
4.3.2.1 Simple RS-232C TTL conversion.....	39
4.3.2.2 Accurate RS-232C TTL conversion	39
4.3.3 <i>Master and Slave Configuration</i>	39
4.4 TRANSDUCER MULTIPLEXING	40
4.5 FINAL DESIGN, CONSTRUCTION AND API	41
CHAPTER 5 EXPERIMENTAL PROCEDURES AND RESULTS	43
5.1 DEPTH PRESSURE SENSOR	43
5.1.1 <i>Experiment 1: Output Linearity</i>	43

5.1.1.1	Aim	43
5.1.1.2	Background.....	43
5.1.1.3	Method	43
5.1.1.4	Results.....	44
5.1.1.5	Analysis	44
5.1.2	<i>Experiment 2: Noise and Electromagnetic Interference (EMI)</i>	45
5.1.2.1	Aim	45
5.1.2.2	Background.....	45
5.1.2.3	Method	46
5.1.2.4	Results.....	47
5.1.2.5	Analysis	49
5.1.3	<i>Experiment 3: Depth Calibration</i>	50
5.1.3.1	Aim	50
5.1.3.2	Background.....	50
5.1.3.3	Method	50
5.1.3.4	Results.....	51
5.1.3.5	Analysis	52
5.2	SONAR MULTIPLEXING SYSTEM	52
5.2.1	<i>Experiment 1: Beam Width and Shadowing</i>	53
5.2.1.1	Aim	53
5.2.1.2	Background.....	53
5.2.1.3	Method	53
5.2.1.4	Results.....	54
5.2.1.5	Analysis	54
5.2.2	<i>Experiment 2: Perpendicular Transducers</i>	55
5.2.2.1	Aim	55
5.2.2.2	Background.....	55
5.2.2.3	Method	56
5.2.2.4	Results.....	56
5.2.2.5	Analysis	56
5.2.3	<i>Experiment 3: Wall Following – Proportional Controller</i>	56
5.2.3.1	Aim	56
5.2.3.2	Background.....	56
5.2.3.3	Method	56
5.2.3.4	Results.....	57
5.2.3.5	Analysis	57
5.2.4	<i>Experiment 4: Wall Following – Fuzzy Logic</i>	58
5.2.4.1	Aim	58
5.2.4.2	Background.....	58
5.2.4.3	Method	58
5.2.4.4	Results.....	61
5.2.4.5	Analysis	61
CHAPTER 6 CONCLUSION AND FUTURE WORK		63
6.1	OUTCOMES	63
6.1.1	<i>Depth Pressure Sensor</i>	63

6.1.2	<i>Sonar Multiplexing System</i>	63
6.2	FUTURE WORK	64
6.2.1	<i>Depth Pressure Sensor</i>	64
6.2.2	<i>Sonar Multiplexing System</i>	64
6.3	FINAL COMMENT	64
APPENDIX A DEPTH SENSOR API		67
APPENDIX B SONAR MULTIPLEXING SYSTEM SCHEMATIC		69
APPENDIX C SONAR MULTIPLEXING SYSTEM API		71
APPENDIX D EMI EXPERIMENT RESULTS - CONTINUED		73
APPENDIX E VOLTAGE REGULATOR		77
APPENDIX F CD-ROM LISTING		79
	APPLICATION PROGRAM INTERFACE (API)	79
	DELIVERABLES	79
	DESIGNS	79
	EXPERIMENTS	79
	MEDIA	79
	PRESENTATIONS	80
BIBLIOGRAPHY		81

Nomenclature

Abbreviations and Acronyms

AC	Alternating Current
ADC	Analogue to Digital Converter
API	Application Program Interface
ata	Atmospheric Pressure, 101.325 kPa = 14.696 psi
AUV	Autonomous Underwater Vehicle
AUVSI	Association for Unmanned Vehicle Systems
bar	100 kPa = 14.504 psi
bps	Bits per second
CMOS	Complimentary Metal-Oxide-Semiconductor
CMRR	Common Mode Rejection Ratio
DC	Direct Current
EMI	Electromagnetic Interference
EyeBot	The central computer controller for the AUV
kPa	Kilopascals, SI unit for pressure, Nm ⁻²
MIT	Massachusetts Institute of Technology
NMEA	The Nation Marine Electronics Association
NMEA 0183	A serial data protocol used in marine equipment
Op Amp	Operational Amplifier
ppt	Parts per thousand
psi	Pounds per Square Inch
psig	PSI Gauge, relative to atmospheric pressure
PWM	Pulse-width Modulation
RMS	Root Mean Square
ROV	Remotely Operated Vehicle
RS-232C	The standard Serial Port protocol used on computers
RX	Receiver
TTL	Transistor-Transistor Logic, Commonly +5V level
TX	Transmitter
UWA	University of Western Australia

Nautical Terminology and Directions

Bow	The front of the AUV
Forward	Towards the front
Stern	The back of the AUV
Aft	Towards the back
Port	Left side of the AUV (when facing forward)
Starboard	Right side of the AUV (when facing forward)

List of Variables

p	Pressure (kPa)
$p_{\text{atmospheric}}$	Atmospheric pressure, 101.325kPa
p_{absolute}	Absolute pressure
p_{gauge}	Gauge pressure, $p_{\text{absolute}} - p_{\text{atmospheric}}$
ρ	Density, $\rho_{\text{water}} = 1000 \text{ kgm}^{-3}$
g	Gravitational Constant, $g = 9.8\text{ms}^{-1}$
h	Distance below water surface (metres)
V	Volume
v	Velocity
s	Displacement
t	Time
T	Temperature (Degrees Celsius)
S	Salinity (parts per thousand)
D or d	Depth (metres)
V_{offset}	Zero-point output of the pressures sensor
K_p	Proportional controller constant

List of Figures

FIGURE 1: SUPER SCORPIO ROV [12].	2
FIGURE 2: UWA'S AUTONOMOUS UNDERWATER VEHICLE (AUV) - <i>MAKO</i> .	3
FIGURE 3: PRESSURE AND VOLUME AT DEPTH [9].	8
FIGURE 4: SENSOTEC TJE-SERIES SENSOR [25]	9
FIGURE 5: GLOBAL WATER INSTRUMENTS WL400 [11]	9
FIGURE 6: MOTOROLA MPX5100DP [15]	10
FIGURE 7: SEA-BIRD SBE 50 [24]	11
FIGURE 8: CHANGES IN TEMPERATURE, SALINITY AND PRESSURE WITH DEPTH [23].	12
FIGURE 9: SPEED OF SOUND IN WATER [23]	13
FIGURE 10: REFRACTION OF SOUND WAVES IN WATER [23]	14
FIGURE 11: NAVMAN DEPTH 2100	17
FIGURE 12: SAMPLE RS-232C SERIAL WAVEFORM FOR 8 DATA BITS, ODD PARITY AND 1 STOP BIT.	18
FIGURE 13: PROPORTIONAL CONTROLLER	21
FIGURE 14: SENSYM SX15GD2, BASED ON PICTURES FROM [27].	25
FIGURE 15: SX15GD2 EQUIVALENT CIRCUIT, A WHEATSTONE BRIDGE	26
FIGURE 16: SENSYM SX-SERIES BRIDGE RESISTANCE AND SPAN VS. TEMPERATURE [27]	28
FIGURE 17: SX-SERIES TEMPERATURE COMPENSATION AND AMPLIFIER CIRCUIT, COLOUR CODED	29
FIGURE 18: FABRICATED DEPTH PRESSURE SENSOR PCB	30
FIGURE 19: DEPTH PRESSURE SENSOR – MECHANICAL DESIGN	32
FIGURE 20: INSTALLED DEPTH SENSOR	34
FIGURE 21: OPPOSING TRANSDUCERS WILL INTERFERE	36
FIGURE 22: SONAR MULTIPLEXING SYSTEM - OVERVIEW	37
FIGURE 23: PICAXE PRODUCT COMPARISON [20].	38
FIGURE 24: SIMPLE RS-232C TO TTL CONVERSION	39
FIGURE 25: TELECOM RELAYS	40
FIGURE 26: FABRICATED SONAR MULTIPLEXING SYSTEM CIRCUIT BOARD	42
FIGURE 27: SIMULATED PRESSURE SENSOR LINEARITY	44
FIGURE 28: FLUCTUATION FILTERING CIRCUIT	46
FIGURE 29: STERN MOTOR, CLOSEST TO THE PRESSURE SENSOR	48
FIGURE 30: BOW MOTOR, FURTHEST FROM THE PRESSURE SENSOR	48
FIGURE 31: PRESSURE SENSOR OUTPUT BEFORE (LEFT) AND AFTER (RIGHT) THE FILTERING CIRCUIT	49
FIGURE 32: MEASUREMENT METHOD AND APPARATUS	51
FIGURE 33: ACTUAL AUV DEPTH PLOTTED AGAINST THE PRESSURE SENSOR READING	52
FIGURE 34: BEAM WIDTH AND SHADOWING SET-UP	53
FIGURE 35: MAPPING OF AN OBSTACLE IN THE POOL	54
FIGURE 36: WALL-FOLLOWING USING A PROPORTIONAL CONTROLLER	57
FIGURE 37: ERROR MEMBER FUNCTION	59
FIGURE 38: ERROR RATE OF CHANGE MEMBERSHIP FUNCTION	59
FIGURE 39: WALL FOLLOWING USING FUZZY LOGIC	61

Chapter 1

Introduction

1.1 Remotely Operated Vehicles (ROVs)

Underwater vehicles, namely (Submersible) Remotely Operated Vehicles or "ROVs", have been used in the offshore mining and exploration industries for around thirty years. Often used in places inaccessible to scuba divers, they routinely carry out tasks from inspecting pipelines to recording environmental data and photographing shipwrecks.

In 1953, photographer Dimiri Rebikoff developed the first known ROV [28]. He termed it "Chien Plongeur" which loosely translates from French to "Plunger Dog". In a Cold War effort by the Americans during the early 1960s, the U.S. Navy developed an ROV. This ROV was later used in 1966 to recover a Nuclear Warhead lost off the coast of Spain. The same model ROV was used again in 1976 to save the lives of two pilots trapped in a sunken submersible vehicle off the coast of Cork, Ireland.

Earlier this year in August 2005 the US Navy used two "Super Scorpio" ROVs to free 30 sailors trapped inside a Russian submarine. At 190m deep, the ROVs were used to cut away a fishing net that had tangled around the propeller of the submarine. The "Super Scorpio" ROVs are capable of reaching a maximum depth of 1500m and cutting 2.5cm steel cable [31].



Figure 1: Super Scorpio ROV [12].

1.2 Autonomous Underwater Vehicles (AUVs)

At the University of Western Australia's Centre for Intelligent Information Processing Systems (CIIPS), *Project Mako* is the ongoing development of an Autonomous Underwater Vehicle (AUV). AUVs represent the next generation in ROV technology. Unlike ROVs that have to be constantly driven by people in a control room onboard the launching ship, as the name suggests, AUVs have the ability to operate autonomously. AUVs will ultimately require far less human control and intervention than the currently used ROVs, making them the likely successor. *Project Mako* aims to develop a platform for which autonomy routines and technology can be tested. Universities all around the world are developing similar AUVs such as the Massachusetts Institute of Technology's (MIT's) ORCA Autonomous Underwater Vehicle. *Mako* very closely resembles the mechanical construction of Cornell University's aptly named "CUAUV" [8]. AUVs built are invited to compete in the Association for Unmanned Vehicle Systems Internationals (AUVSI's) annual International Autonomous Underwater Vehicle Competition (IAUVC) [3]. AUVs competing in this competition are scored on their ability to perform tasks that simulate the real-life activities of an AUV. These tasks include pipeline following and object detection.

1.3 Project Mako

At the commencement of this project, the AUV *Mako* had the following specifications:

- EyeBot MK4 controller (33MHz);
- Cyrix microATX PC (233MHz/32MB/5GB) for image processing;
- infrared for controlling the EyeBot;
- Bluetooth for sending and receiving data from the EyeBot;
- WiFi Access Point for accessing the Cyrix PC;
- Navman Depth 2100 sonar in the forward and downward directions;
- Navman Speed 2100 speed sensor;
- electronic compass;
- aluminium frame, painted with Chrysler metallic blue paint;
- three 12V batteries totalling 31Ah; and,
- a total mass in excess of 35kg.

A photo of the AUV *Mako* is shown below in Figure 2.

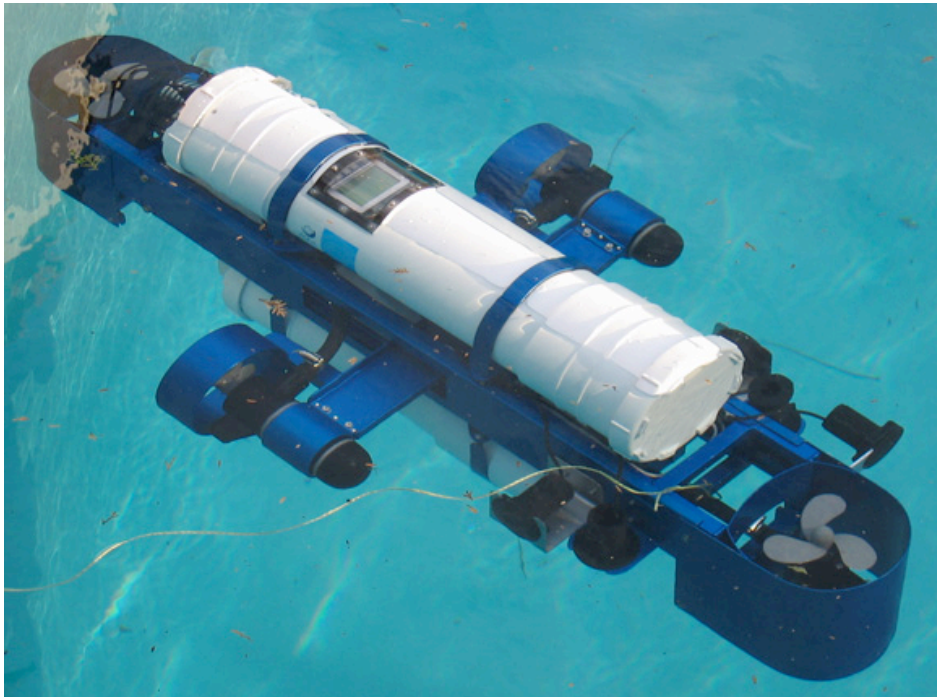


Figure 2: UWA's Autonomous Underwater Vehicle (AUV) - *Mako*

1.4 Project Motivation

Following on from the work completed by the foundation *Project Mako* team in 2004, there remained areas suggested for improvement in order for *Mako* to be a fully functional AUV. These areas include:

- the incorporation of a depth sensor;
- the addition of left and right sonar to enable wall-following and better collision avoidance;

- the development of a better thrust-based control system for the motors;
- the integration of inertial sensors for better control; and,
- improvement in the accuracy of the velocity sensor.

This project addresses the first two of these – the incorporation a depth sensor and the addition of left and right facing sonar.

1.4.1 The Depth Pressure Sensor

The first objective of this thesis project is to implement a depth pressure sensor to enable the AUV *Mako* to maintain a desired depth underwater or "hover". To do this the EyeBot controller must be able to instantaneously measure the depth of the vehicle. As the depth of the vehicle increases, the weight of the water above exerts a linearly increasing force known as the "hydrostatic pressure" on the vehicle. Through the addition of a pressure sensor to measure the hydrostatic pressure, the depth of the vehicle can be determined with remarkable speed and accuracy. The first aim of this thesis project is to develop this depth pressure sensor and incorporate it on the AUV *Mako*.

1.4.2 The Sonar Multiplexing System

Continuing the work of Minh Nguyen [18], the second objective of this thesis project is to implement a working sonar telemetry system on the AUV. Minh Nguyen conducted experiments last year with the LM1812 integrated ultrasonic transceiver controller. However, the Electronics Workshop has since advised that these integrated circuits are no longer in production and no suitable replacements are available to complete Minh Nguyen's design [18]. Due to the obsolescence of the LM1812, the existing Navman Depth 2100 systems incorporated on the AUV *Mako* will be further developed in order to improve their functionality and reliability.

For the Navman Depth 2100, a basic single-direction sonar system consists of an acoustic transducer (like a speaker and microphone in one), and a sonar controller that processes the signal from the transducer. The controller outputs the measured distance, at 1-second intervals, as text data that *Mako's* EyeBot controller can read. Prior to the commencement of this project, the AUV *Mako* had two Navman sonar transducers (one facing the forward and one facing down) and one Navman sonar controller that could be manually connected to either of these two transducers. The

aim of this second objective is to install new left and right-facing transducers and to develop a multiplexing system to interface all of these sensors to the EyeBot controller.

1.5 Thesis Outline

Chapter 1: This chapter introduces Autonomous Underwater Vehicles and *Project Mako*. It presents the overall aims and motivation of this thesis project.

Chapter 2: This chapter introduces the relevant background theory along with methods used by AUVs around the world. The theory relevant to the depth pressure sensor is introduced first, followed by the information relevant to the sonar system.

Chapter 3: This chapter details the methodologies behind the design of the depth pressure sensor. It builds on the theory and background information established in Chapter 2.

Chapter 4: This chapter details the methodologies behind the design of the sonar multiplexing system, again building on the theory and background information established in Chapter 2.

Chapter 5: This chapter details the experiments conducted on both the depth sensor and sonar multiplexing system. It provides numerical measurements, along with analysis and discussion of the results obtained.

Chapter 6: This chapter summarises the outcomes of this thesis project and suggests possible future work for *Project Mako*.

Chapter 2

Background Theory and Technologies

There is a certain amount of background theory necessary to understand how the depth pressure sensor and sonar multiplexing systems work. The relevant information will be introduced in this chapter along with methods used by AUVs around the world at other universities. The theory relevant to the depth pressure sensor will be introduced first, followed by the information relevant to the sonar system.

2.1 Pressure, Fluid Pressure and Depth

2.1.1 Units of Pressure

The SI units for pressure are kilopascals (kPa). Atmospheric pressure is approximately 101.325 kPa at sea level. Although kPa are the SI units for pressure, when dealing with air pressure it's common to use the units "atmospheres" (ata) and "bar" (bar). One atmosphere (1 ata) of pressure is 101.325 kPa and one bar (1 bar) of pressure is 100 kPa. Due to the small numerical difference between these values, atmospheres and bar are often considered equal.

The imperial units for pressure are pounds per square inch (PSI). Atmospheric pressure is approximately 14.696 psia. The "a" at the end of the units is a convenient way of noting that the value is an "absolute pressure". This is opposed to 14.696 psig, where the "g" denotes "gauge pressure". Gauge pressure is pressure relative to atmospheric pressure according to the following relationship:

$$P_{psia} = P_{psig} + 14.696$$

The units "psig" are commonly seen when dealing with pressure transducers as most manufacturers are American and most applications require pressure measurement relative to atmospheric pressure.

2.1.2 Hydrostatic Pressure and Pascal's Law

Hydrostatic pressure is the force exerted on an object due to the weight of fluid (in this case water) present above it [7]. It follows a relationship known as Pascal's Law:

$$p = \rho gh + p_{atmosphere}$$

Where p is pressure in Pa, ρ (rho) is the fluid density (1000kgm⁻³ for fresh water), g is the gravitational constant (9.8ms⁻¹) and h is the depth below the fluid (water) level. Hydrostatic pressure is an isotropic force, which means the force exerted on the object is equal from all directions.

2.1.3 Boyle's Law

Boyle's Law states that the pressure-volume product for a given gas (such as air) is constant [4]. That is:

$$pV = k$$

Where V is the volume occupied by the gas at pressure p and k is a constant. This law can be used to relate the pressure and volume of a gas before and after it has undergone a change, according to the following relationship:

$$p_1V_1 = p_2V_2$$

Where the subscript 1 denotes before the change and subsequently the 2 corresponds to after.

2.1.4 Pressure at Water Depth

Based on these principles of hydrostatic pressure and Boyle's Law, a volume of air at depth underwater can now be considered. According to Pascal's Law, the pressure at a water depth of 10.33m will be 202.6kPa, double that of atmospheric pressure. Further, according to Boyle's Law, if a volume of air were trapped in a flexible container at atmospheric pressure, once lowered to a depth of 10.33m the volume would be halved due to the doubling of pressure. This is evident in Figure 3 where atmospheric pressure (1 ata) has been assumed to be 100kPa (1 bar) and the gravitational constant has been rounded to 10ms⁻² for simplicity.

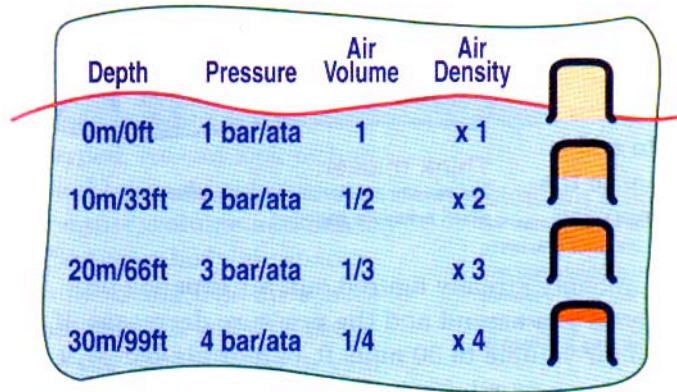


Figure 3: Pressure and Volume at Depth [9].

2.2 Depth Pressure Transducers and Sensors

Utilising these principles of hydrostatic pressure and Boyles Law to measure water depth, there are a variety of pressure transducers and sensors currently used on research and commercial ROVs and AUVs.

2.2.1 Research AUVs

Research institutions such as Cornell University, Massachusetts Institute of Technology (MIT), Duke University, Curtin University of Technology and the United States Naval Academy employ the following different pressure transducers and sensors on their AUVs.

2.2.1.1 Sensotec TJE-series Pressure Sensor

Cornell University's "CUAUV" [8] and MIT's "ORCA-VII" [2], among others, use Honeywell/Sensotec TJE-series pressure sensors. The TJE-series sensors have the following benefits when used in this application [25]:

- the ability to directly accept an ionic wet fluid (eg. water) at the input port;
- a stainless-steel construction for corrosion-resistance;
- accuracy to 0.1%;
- analogue output for infinite resolution and sampling rate;
- temperature compensation for varying water temperatures;
- gauge-type sensing (the output relative to atmospheric pressure); and,
- internal amplification and calibration circuitry.

Shown in Figure 4, at the time of writing, these units retail for around \$US300 for the less expensive un-amplified model.



Figure 4: Sensotec TJE-series sensor [25]

2.2.1.2 Global Water Instruments WL400 Transducer

Duke University's "Charybdis" AUV [10] uses a WL400 submersible water level transducer, manufactured by Global Water Instruments. This has similar specifications [11] to the TJE-series sensors however its output is un-amplified. Being a transducer, the output is in the form of an output current between 4 and 19mA. The datasheet recommends using a 125Ω resistor in parallel with the transducer (rather than a transimpedance amplifier) to give an output voltage rather than a current. Shown in Figure 5, at the time of writing, these transducers retail for approximately \$US495.



Figure 5: Global Water Instruments WL400 [11]

2.2.1.3 Motorola MPX5100DP

Curtin University of Technology along with the United States Naval Academy (USNA) [30] have selected the Motorola MPX5100DP [15] pressure sensor to provide depth measurement. Unlike the Global Water Instruments and Sensotec sensors previously introduced, this sensor is not recommended for use with wet input fluids like water. To overcome this limitation, Curtin University of Technology use a coiled hose to trap air between the sensor and the surrounding water while USNA appear

to disregard this recommendation. The MPX5100DP does have an inbuilt amplifier with temperature compensation circuitry to directly provide a 0-5V output radiometric to the supply voltage. The accuracy of this sensor however is only 2.5%. This is much less accurate than the previously introduced sensors. Shown in Figure 6, an equivalent sensor is manufactured by Freescale Semiconductor and is readily available in the United States for approximately \$US20.



Figure 6: Motorola MPX5100DP [15]

2.2.2 Commercial ROVs and AUVs

Companies developing commercial ROVs and AUVs often don't release specific information regarding particular components they're using as these may often change with availability and be dependent on the application of the vehicle. Sea-bird Engineering, Inc, developed a turnkey solution for depth pressure sensing on ROVs and AUVs.

2.2.2.1 Sea-bird SBE 50 Digital Oceanographic Pressure Sensor

One such pressure sensor designed for use in commercial remotely operated and autonomous underwater vehicles is the Sea-bird SBE 50 (pictured in Figure 7). This series of pressure sensors has the following specifications [24]:

- fully submersible to 7000m, with a waterproof bulkhead connector;
- Titanium construction for corrosion-resistance and strength;
- accurate to 0.002%;
- analogue (0-5V) and 16Hz sampled RS-232C serial output;
- temperature compensation for varying water temperatures; and,
- internal amplification and calibration via its microcontroller.

Comparing this sensor to those used on current research AUVs, it has a much higher accuracy and depth rating, a Titanium construction as opposed to stainless steel or plastic, and it features an inbuilt microcontroller for calibration and direct RS-232C serial data communication. It can also be configured via management software to

average its output over multiple samples and to act passively rather than actively. That is, in passive mode it only will return the depth when queried, rather than continuously (actively) at 16 samples per second. This completely integrated package aims to be a simple plug-and-play depth pressure sensor for AUV and ROV designers to incorporate into their vehicles. The SBE 50 is introduced here to allow comparison between cutting edge depth sensing technologies and those more realistically obtainable.



Figure 7: Sea-bird SBE 50 [24]

2.3 Sonar and Distance Measurement

2.3.1 Passive and Active Sonar

There are two main types of sonar - passive sonar and active sonar. Firstly, passive sonar is the where the sonar transducers simply listen for sounds. Passive sonar is mainly used for scientific and military purposes. Passive sonar often involves mathematically interpreting the acoustic wave patterns received by multiple hydrophones (underwater microphones) in order to establish the bearing of the received sound. Passive sonar may also be used in conjunction with mathematical matching algorithms to estimate the source causing the sound. For example, the electrical transformers on U.S. submarines will need to operate at the U.S. AC mains line frequency of 60Hz in order to provide power to computer equipment and lighting. If these transformers are not sufficiently acoustically dampened or isolated from the shell of the submarine, this 60Hz "hum" can be used to identify the submarine and pinpoint its bearing [19]. This "hum" forms part of the acoustic signature of the submarine. The U.S. Office of Naval Intelligence maintains a computer database of the acoustic signatures of various sounds such as torpedos being launched [19]. This gives the military the ability to quietly and undisruptively identify and locate other objects underwater.

The second more common form of sonar is active sonar. Active sonar involves transmitting a "ping" (short pulse of acoustic energy) and recording the arrival times of the resulting backscattered pings. Based on the time taken for the reflected ping to return to the transducer, the distance of the object that caused the reflection can be calculated due to the velocity of sound in water being a well-defined function.

2.3.2 Principles of Active Sonar

2.3.2.1 Speed, Distance and Time

As introduced previously, active sonar involves sending out a "ping" or burst of sufficiently powerful acoustic energy from a transducer, and timing how long it takes for the sound to be reflected and reach the transducer again. Where the same transducer both sends and receives the "ping" this geometry is termed monostatic. Where the sending and receiving transducers are separate and in separate physical locations the geometry termed bistatic. For the purposes of this thesis, only the monostatic case will be considered. It is however worthwhile to note that other configurations are possible and often useful.

Take the classical Newtonian relationship for constant velocity, distance and time

$$s = vt$$

where s is displacement in meters, v is velocity in meters per second, and t is time in seconds. With the ping return-trip time t known, the last quantity required to solve for the displacement s is the velocity v of sound in water. The velocity of sound in water is dependent on the temperature, salinity and either pressure or depth of the water. For the case of water half way between the equator and the South Pole (Australia), approximate profiles of these relationships are shown in Figure 8.

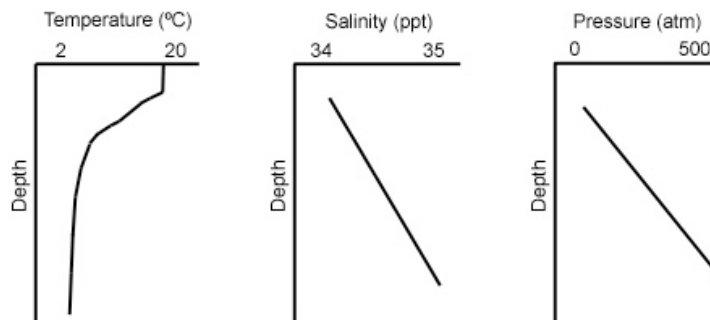


Figure 8: Changes in temperature, salinity and pressure with depth [23]

When these relationships in Figure 8 are combined, a profile develops for the speed of sound in water at depth. An example of this profile is shown in Figure 9. The dotted lines at certain depths represent the boundaries between areas where different effects dominate.

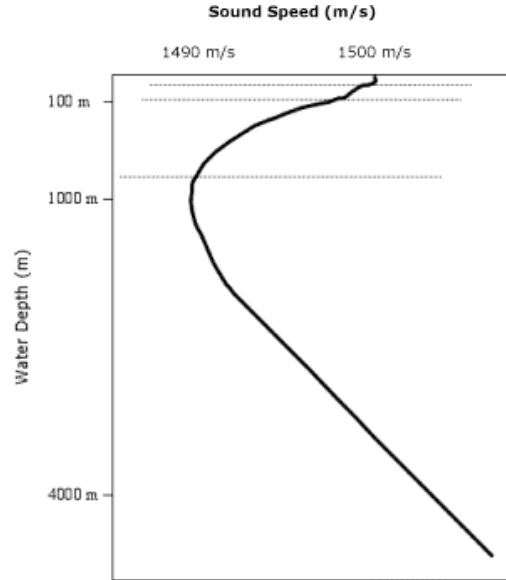


Figure 9: Speed of sound in water [23]

The velocity of sound in water at a given depth is commonly described by the UNESCO equations [1] that form an algorithm for determining the velocity of sound in water for a given temperature, salinity and pressure. For simplicity, various approximations to this algorithm exist with different ranges of validity. One such approximation is the Coppens' relationship [1]:

$$v(D,S,T) = v(0,S,T) + (16.23 + 0.0253T) \left(\frac{D}{1000} \right) + (0.213 - 0.01T) \left(\frac{D}{1000} \right)^2 + 0.1 [0.016 + 0.0002(S - 35)] (S - 35) T \left(\frac{D}{1000} \right)$$

$$v(0,S,T) = 1449.05 + 4.57T - 0.0521T^2 + 0.00023T^3 + (1.333 - 0.0126T + 0.00009T^2)(S - 35)$$

Where v is the sound velocity, D is depth in metres, S is salinity in parts per thousand and T is temperature in degrees Celsius. This relationship is valid for temperatures from 0 to 25°C, salinity from 0 to 24ppt and depth from 0 to 4000m.

With current ROV and AUV technology able to reach depths of around 2000m, these changes in water sound velocity become important if sonar is to be useful for mapping the ocean floor and locating deep shipwrecks. The maximum sound speed difference of 10kmh⁻¹ (from Figure 9) is not directly the problem, but rather the speed gradient that exists in the water. This gradient results in the sound path bending, similar to how sound bends at night due to the changing air density gradient, and

how light refracts at a refractive index boundary. This is shown in Figure 10. Section (A) shows the refractive index profile of the water and (B) shows the semi-sinusoidal path of travelling sound waves.

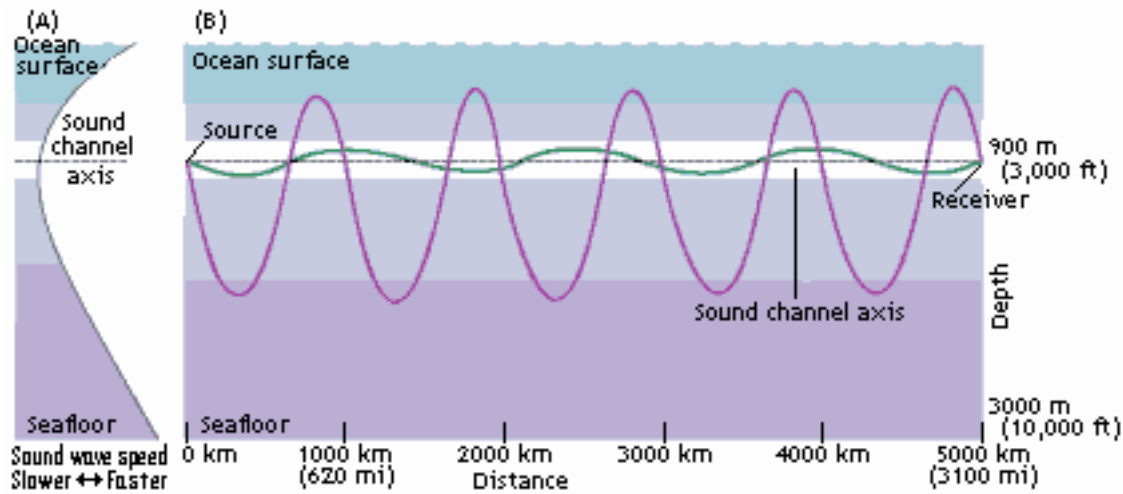


Figure 10: Refraction of sound waves in water [23]

In the pool and at the depths that current University's AUVs travel, this refraction of sound is not going to be a problem. However, unlike submarines and ROVs, as humans do not directly drive AUVs, onboard sensors will need to be used to locate targets underwater. When using sonar to find these targets (like pipes or well-heads) over long distances autonomously underwater, acoustic refraction will render active sonar problematic. Thus other sensing technologies like stereo vision and underwater GPS [16] via acoustic beacons will be critical for long-range telemetry.

Shown in Figure 8, water exhibits a unusual temperature profile. This has implications for the depth sensing circuitry on AUVs and ROVs. The pressure transducer amplifier must be able to compensate for the changes in water temperature in order to maintain acceptable accuracy. Note from the graph in Figure 8 that water close to the surface is around 18°C. This is due to the wind and waves agitating the water, with sunlight warming the water at the surface. Before 100m deep, water undergoes a sharp change in temperature. This sharp change is known as the thermocline. Scuba divers can often notice an abrupt change in the temperature of the surrounding water in depths around 20m. To scuba divers looking downward from above, the thermocline will often appear like a layer of

opaque glass below them. After the thermocline has been reached, water temperature decreases rapidly as sunlight fails to reach the depth.

2.3.2.2 Finite Power

To this point it has been assumed that the "ping" transmitted by active sonar has sufficient power such that the reflected ping returns to the transceiver. Thus, for a sonar system to work, a fundamental inequality exists. The received signal level must exceed the losses and any background signal levels. Assuming the sonar system is monostatic (transducer sends and receives), there are three main influences on the signal levels [18]:

- The Equipment:
 - Source Level (SL) or transmitted acoustic energy at 1 metre;
 - Directivity Index (DI) or how focused the transducer is; and,
 - Detection Threshold (DT) or how sensitive the receiving system is.
- The Medium:
 - Transmission Loss (TL) or one-way energy loss in the medium;
 - Reverberation Level (RL) or noise from backscattered pings; and,
 - Noise Level (NL) or isotropic noise from wind, waves, etc.
- The Target:
 - Target Strength (TS) or how well the target reflects the ping.

As the Reverberation Level (RL) generally exceeds the Noise Level (NL) so we will omit the Noise Level (NL) as it does not dominate. When these quantities are all in decibels (dB) the following additive relationship exists [18]:

$$SL + DI + TS - 2TL - RL \geq DT$$

It is evident from this equation that the left-hand side must be greater than or equal to the right-hand side for the ping to be successfully detected. This power budget calculation can indicate whether a sonar system will be effective in a given environment and over what distance.

2.3.2.3 Multipath Fading

For University developed AUVs, one of the most major problems facing sonar is multipath fading. Multipath fading, or simply multipath, is where sonar pings may

travel from one transducer over multiple different paths before arriving back at the transducer to be received. Multipath is the largest source of sonar measurement error in shallow water (small-scale propagation) environments where the walls and objects surrounding the transducer are flat surfaces (on the scale of the wavelength) with high target strengths (high reflectivity). Pools fit into this small-scale propagation category.

In pools, the reflected sound-wave power levels are sufficiently high that significant constructive and destructive interference patterns can occur. This can result in the situation where multipath waves destructively interfere with the legitimate reflected wavefronts to form a node at the receiver with a power level below the detection threshold (DT). As a result, the legitimate sonar reflection will not be detected and as time passes, further wave interference will cause an antinode above the detection threshold (DT) to occur at the receiver. Thus, the round-trip time will be greater than it should be, resulting in an inaccurate reading. This moving wave formed from the superposition of the multipath waves is where the term fading is derived and gives rise to other effects such as multipath shadowing [21].

Unsurprisingly, multipath fading is essentially a characterisable source of noise. The amplitudes of the signal plus the noise can be predicted by the Raleigh distribution [21]. However, in this small-scale propagation environment, the signal amplitudes are close in magnitude to the noise amplitudes, thus the situation is more accurately characterised by the less common Rician distribution. Unlike the Raleigh distribution, the Rician distribution characterises signals where the noise vector amplitudes are closer to the signal vector amplitude [21].

Modern sonar and underwater acoustic communication systems use complex algorithms, filters and multi-static receivers in order to combat multipath problems. However, these are not always successful. Particularly when the noise power levels approach the signal power levels like in the small-scale propagation case. The best environment for sonar is open water. Multipath reflections will be limited in both quantity and power due to the absence of all-encompassing objects and flat surfaces such as walls. The objects and surfaces that do exist, such as the sandy bottom and

vegetation, will reflect more evenly in all directions (scatter) as they're not as hard and evenly flat on the scale of the wavelength.

The Navman Depth 2100

The Navman Depth 2100 is a boat "echo sounder" system that has been incorporated into the *Mako* AUV in 2004 by Minh Nguyen [18] to provide forward and downward sonar. Typically echo sounders are used to measure and/or map the ocean floor and water depth below boats in open water environments. The Navman Depth 2100 system has the following specifications [17]:

- 0.4m to 180m depth measurement;
- 12V, 100mA power requirements;
- 0.05mV RMS at 60m electrical sensitivity;
- 36W RMS transmitter power;
- 200kHz, 1900pF, 600W transducer;
- 1Hz sampling speed; and,
- NMEA 0183 serial data input/output.



Figure 11: Navman Depth 2100

One Navman Depth 2100 system consists of two separate components; the Navman Depth 2100 controller; and, a through-hull transducer connected by Phono RCA connectors. These components are pictured and labelled in Figure 11.

2.4 Serial Data Communication

2.4.1 Serial Communication

The most common classical serial ports (COM1, COM2, etc.) found on computer systems are described by the RS-232C serial interface standard. A standard that is fast becoming antiquated by the evolution of higher-speed Universal Serial Bus (USB) technology, RS-232C serial communication is still very commonly used in the

robotics industry because of its simplicity. For the purposes of this thesis, a brief overview of the RS-232C serial standard will be given, describing only what is necessary to understand simple serial communication. The information to be presented here on serial communication is adapted from the paper *Serial Data Transmission* from Samson AG [22].

2.4.1.1 Electrical Connection

Most simply, RS-232C serial links between two devices have three important wires. These are: the data-receiving wire (RX); the data-sending wire (TX); and, the signal ground wire (GND). The signal ground wire exists to create a common voltage reference for the two devices in order to construct a potential difference at the data wires. The RX and TX voltage levels required for RS-232C serial communication are evident in the example serial waveform shown in Figure 12. By current standards, the decision boundary for determining the state of a bit is $\pm 3V$, with maximum loaded bit voltage of $\pm 15V$.

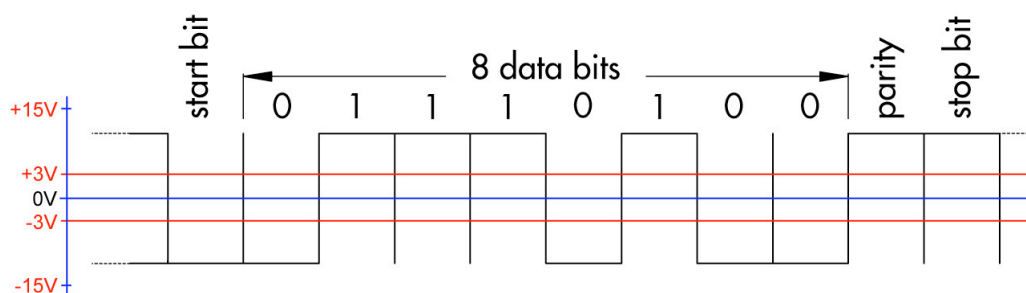


Figure 12: Sample RS-232C serial waveform for 8 data bits, odd parity and 1 stop bit.

Microcontrollers and other digital CMOS and TTL circuitry commonly operate at 0V for logical 0 and +5V for logical 1. This means that transposition circuitry is needed to interface RS-232C serial devices with TTL and CMOS devices like microcontrollers.

2.4.1.2 Start and Stop Bits & Baud Rate

RS-232C serial is an asynchronous technology. That is, the sender and receiver need to synchronise without the aid of a clock pulse defining where the bits occur. To do this, the receiver needs to be able to identify where the sequence of data (like in Figure 12) starts, and the duration of each bit.

Identifying the start is achieved using the start and stop bits shown. The RS-232C standard specified that the user must choose the stop bit to be 1, 1.5 or 2 bits in duration.

The duration of the bits is determined by the "baud rate" of the serial communication. Common baud rates for serial data are 4800, 9600 and 115200bps although many others exist.

2.4.1.3 Parity

The parity bit is used for error detection in the transmitted message. For the case in Figure 12, odd parity is used. For odd parity, the value of the parity bit is selected so that the number of 1s sent (including the parity bit) is odd. The RS-232C standard specifies that the user must choose odd, even or no parity.

2.4.1.4 Data Bits

Eight data bits are used in the above signal. This is the most common value, however, the user may choose from 8, 7, 6 or 5. Obviously the shorter the number of data bits, the more likely the sender and receiver will remain synchronised during the communication time as the start and stop bits will occur more frequently. This comes at the cost of more overhead, as start and stop bits, essentially containing no data, will occur more.

2.4.1.5 Sender and Receiver Configuration

It should be evident that the receiver and the sender must be configured with the same parameters (baud rate, data bits, parity and stop bit duration) for the data sent over a serial link to be correctly received.

2.4.2 The EyeBot Controller

The University of Western Australia's AUV *Mako* uses a fourth generation EyeBot controller for its main input/output and computational operation. The EyeBot is a flexible, simple and easy to program (C/C++) controller that has the ability to manage all of the digital input/output and sensor connectivity required on the AUV.

The EyeBot M4 has three serial ports - one at RS-232 level ($\pm 15V$) and two at TTL level ($\pm 5V$). The serial port at RS-232 level is the program download port, which is currently used for Bluetooth communications. The second TTL level serial port is currently used for the Navman Depth 2100 controller and the third port is unconnected.

2.4.3 The NMEA 0183 Protocol

NMEA 0183 is a protocol developed by the National Marine Electronics Association (NMEA) for the networking of navigational equipment on marine craft. NMEA 0183 networks consist of "talkers" and "listeners". NMEA 0183-compatible GPS receivers, depth gauges and fuel monitors are examples of "talkers" as they send out serial data to be received by "listeners" such as autopilot driving systems that use this data to steer the vessel. Essentially NMEA 0183 uses EIA-422 to send and receive serial data at 9600 baud, with 8 data bits, no parity and 1 stop bit. EIA-422 is essentially the same as RS-232 however it uses twisted-pair cable (like Ethernet) to allow for longer cable lengths. EIA-422 and RS-232 equipment is designed by specification to be practically interchangeable, thus EIA-422 NMEA 0183 equipment can generally be directly connected to any RS-232 serial port.

The Navman Depth 2100 controllers used in the sonar system of the AUV are NMEA 0183 compliant. Below is an example of the serial data "sentences" sent out by the Navman Depth 2100 "talker":

```
$SDDPT,0.4,0.0,*7F  
$SDDPT,0.4,0.0,*7F  
$SDDPT,0.2,0.0,*7D
```

Breaking the first one of these sentences into its comma delineated parts, the \$SDDPT token indicates the sentence originates from a depth sounder. The following two decimal numbers indicate the current depth (0.4) followed by the offset between the depth reading and the lowest point on the boat (0.0). Finally, the asterisk (*) denotes "hexadecimal checksum" where 7F is the hexadecimal checksum of this sentence. This checksum is determined from the bit-wise exclusive-OR of all of the other data in the sentence contained between, and excluding, the dollar (\$) and the asterisk (*).

2.5 Control Theory

2.5.1 Proportional or P-Control

Proportional (or simply P) control is the most basic simplification of the Proportional-Integral-Derivative (PID) controller. Often used in robotics and the engineering industry, controllers like this utilise feedback from a process to ensure stable control. A signal flow diagram of a P-controller is shown in Figure 13.

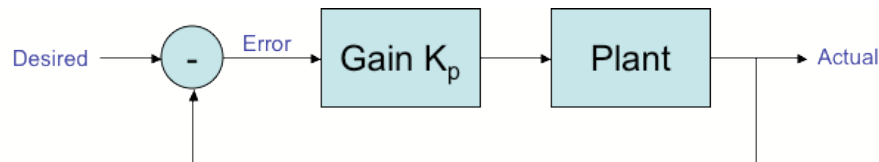


Figure 13: Proportional controller

To explain how the P-controller in Figure 13 works, it is useful to consider an example process. Take the speed regulation of a motor under varying load. As the load increases, the power supplied to the motor will need to increase in order to maintain the same desired velocity. The P-controller works by subtracting the actual speed (determined by a supporting feedback mechanism such as a tachometer or rev. counter) from the desired speed of the motor. The resulting "error" value is then scaled by a constant known as the proportional constant, K_p , and used to adjust the power to the motor. If the constant K_p is too large, oscillations can occur as the P controller will continually overcompensate for the changed load. If the constant K_p is too small, the P controller will have little or no effect on the speed regulation of the motor. Tuning must be undertaken to ensure that a useful value for the Proportional constant, K_p , is chosen.

2.5.2 Fuzzy Logic

Fuzzy Logic [6] was introduced by Lotfi Zadeh and takes an alternative, non-Boolean and more descriptive, approach to process control theory. Fuzzy Logic is a form of artificial intelligence that attempts to mimic the logical thought processes of human beings.

A common example used to illustrate Fuzzy Logic is that of a person standing in a doorway. In traditional Boolean or binary logic, the person would either be in the kitchen (1) or the living room (0). In Fuzzy Logic the person would be considered to

be in an intermediate state, comprised of their specific membership to each of the rooms - e.g. 30% in the kitchen and 70% in the living room. Further Fuzzy Logic concepts, including the implementation of Fuzzy Logic controller for wall following, will be covered in Chapter 5.

Chapter 3

Depth Pressure Sensor Design

This chapter will detail the methodologies behind the design of the depth sensor by building on the background theory and information already established in Chapter 2.

3.1 Importance of Depth Sensing

All AUVs and ROVs built have a pressure sensor for measuring their instantaneous depth below the surface of the water. It is arguably the most important sensor for underwater vehicles, regardless of their function. When integrated, the depth sensor will provide:

- instantaneous measurements of current depth below the surface of the water;
- protection of the vehicle from damaging water depths/pressures; and,
- the ability to "hover" at a desired depth using closed-loop control of the vertical thrusters.

Through the instantaneous measurement of the current depth of the AUV *Mako*, the AUV can be protected from damaging pressures at depths below the maximum ratings of its components. Louis Gonzales [13] has estimated the absolute maximum depth of the AUV to be around five metres with the motors being the most likely first point of failure. The o-rings, providing the seal around the motor shaft between the wires inside and the surrounding water, are likely to be displaced at pressure. Measures could be taken to overcome this limitation. One such method would be filling the motors with a non-ionic, non-compressible, substance such as mineral oil. This technique is utilised in submersible bore pumps. Another common method for AUVs and ROVs is using motors with a magnetic propeller coupling. For now, the AUV will not be travelling any deeper than five metres, so at this point it is not a problem.

Instantaneous measurement of the current depth, combined with a suitable software control strategy such as PID or Fuzzy Logic, will give *Mako* closed-loop depth control. That is, the ability to "hover" underwater at a desired depth. The AUV is

approximately 4.3% positively buoyant by weight, meaning it naturally floats up to the surface with a force of 15.1N. This positive buoyancy is essential so that in the event of a power or mechanical failure in deep water the AUV won't sink to the bottom. Using the pressure sensor, and a suitable control strategy and the vertical thrusters, this force can be counteracted so that the AUV remains underwater when diving, rather than floating up to the surface continually. Hovering ability is essential for the AUV to remain vertically stable while driving and performing tasks underwater.

This project will essentially focus on the hardware design of the pressure sensor required to produce this functionality. The design and implementation of the software depth controller for *Mako* will form part of Chris Thorp's project, *A Control System for an Autonomous Underwater Vehicle* [29].

3.2 Design Requirements and Aims

The overall aim of the depth pressure sensor design was to produce a depth sensor with accuracy comparable to the expensive commercial AUV depth sensors. As wet pressure transducers are far more expensive than air pressure transducers of the same accuracy, adapting an air pressure transducer for use in the wet environment will achieve this. The overall design of the depth pressure sensor sought to fulfil the following requirements:

- 0 to 4.9V output voltage for direct connection to a port on the EyeBot's analogue to digital converter (ADC);
- an output voltage precisely linearly proportional to pressure;
- an analogue output for infinite sampling speed;
- 0 to 15psig pressure rating – corresponding to 0 to 10m depth;
- <1% accuracy over a wide range of temperatures;
- ease of accurate calibration;
- the ability to be easily adapted for higher pressures and commercial application;
- waterproof, small, lightweight and easily mountable on *Mako*;
- low power consumption for battery operation; and,
- as best value economically as possible.

3.3 Pressure Transducer – SenSym SX15GD2

3.3.1 Specifications and Features

Given the requirements just detailed, an appropriate pressure transducer was selected from the Farnell InOne catalogue (the local specialist electronics retailer). The transducer chosen was the SenSym SX15GD2 [27] pictured in Figure 14.

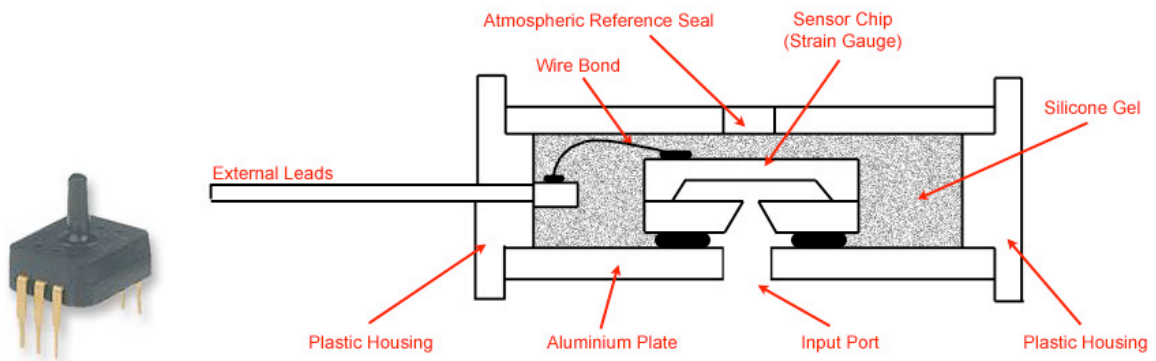


Figure 14: SenSym SX15GD2, based on pictures from [27].

The SX15GD2 low cost, gauge-type, air pressure transducer is designed to operate under pressures from 0 to 15psig (101.325kPa to 206.842kPa i.e. 0m to 10m). As it is a gauge-type pressure transducer it has an internal reference sealed at atmospheric pressure (101.325kPa) resulting in a zero-point output when resting air at sea level. This structure is evident in Figure 14 above where the sensing element is a strain gauge forming a diaphragm as it is suspended between the input port and the sealed atmospheric pressure reference.

The SX15GD2 transducer features low power consumption for battery operation, a typical un-amplified accuracy¹ of 0.2% and a linear temperature response. Unlike the SenSym SDX and higher series of transducers, this SX unit doesn't internally compensate for temperature variation so the external excitation and amplification circuit must.

¹ Quoted from the datasheet [27], represents a combined figure for linearity and hysteresis.

3.3.2 Electronic Characteristics

3.3.2.1 Equivalent Circuit - Semiconductor Wheatstone Bridge

Electronically the transducer is a semiconductor Wheatstone Bridge forming a strain gauge. The equivalent circuit is shown in Figure 15. From the physical construction in Figure 14 the sensor chip is a flexible strain gauge sealed between two volumes of different pressure. When the pressure is equal on both sides of this diaphragm or strain gauge, i.e. when the internal reference (1 ata) is equal to the port pressure (1 ata), there is no deformation force exerted on the bridge and it will be at its zero-point output voltage, V_{offset} . Once the input port pressure, P , begins to increase, the diaphragm strain gauge begins to deform, changing the resistance of the resistors in the Wheatstone Bridge by ∂R . This results in the output voltage, V_{out} , increasing linearly with the input port pressure according to the equation:

$$\begin{aligned} V_{out} &= \frac{\partial R}{R} \times V_{bridge} + V_{offset} \\ &= S \times P \times V_{bridge} + V_{offset} \end{aligned}$$

where ∂ is a constant, S is the sensitivity of the transducer in V/V per kPa and V_{bridge} is known as the bias voltage of the Bridge.

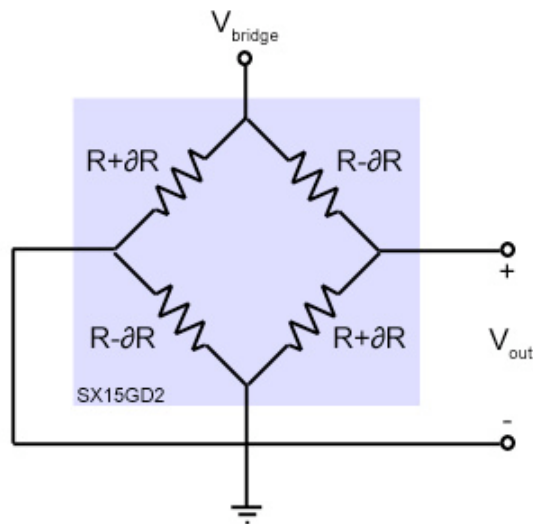


Figure 15: SX15GD2 equivalent circuit, a Wheatstone Bridge

3.3.2.2 Temperature Characteristics

Changing temperature has two main effects on the output of Wheatstone Bridge pressure sensors like the SenSym SX15GD2. Firstly, the more simple effect is where the resistance, R , of all the resistors in the Wheatstone Bridge increases linearly with

temperature. A plot of this relationship for the SX-series of pressure sensors is shown in Figure 16. According to the equation previously introduced for V_{out} ,

$$\begin{aligned}V_{out} &= \frac{\partial R}{R} \times V_{bridge} + V_{offset} \\ &= \partial \times V_{bridge} + V_{offset}\end{aligned}$$

if the value of the resistors in the bridge R changes by an amount Q Ohms, then the following equation will result:

$$\begin{aligned}V_{out} &= \frac{\partial(R+Q)}{(R+Q)} \times V_{bridge} + V_{offset} \\ &= \partial \times V_{bridge} + V_{offset}\end{aligned}$$

Thus, for a constant V_{bridge} , if all of the resistors change value equally, this will have no effect on the output voltage, V_{out} .

If a constant current, I_{bridge} , rather than a constant regulated voltage, V_{bridge} , is used to excite the Wheatstone Bridge then the voltage V_{bridge} will no longer be independent of the resistance of the Bridge elements, R . Thus V_{out} will now change with temperature as V_{out} it is directly proportional to V_{bridge} from the previous equations.

The second temperature dependent effect that occurs is far less simple to characterise and requires nontrivial compensation circuitry to overcome. The problem is that as temperature increases, all pressure sensors become less sensitive. It is as if the silicon diaphragm containing the strain gauge gets stiffer with increasing temperature [26]. This effect is not linear like the first effect, and as a result, it is far more complex to compensate for in circuitry. The difference between the highest and lowest output of a transducer is known as the "span". The span of a sensor is dependent on its sensitivity and hence the body of theory governing this effect is known as "span compensation". The Span vs. Temperature response for the SenSym SX15AD2 is shown in Figure 16.

Varying the Bridge bias voltage can overcome this sensitivity change. Thus the V_{bridge} versus temperature response for constant current excitation can be used to provide temperature compensation if the excitation current is varied by an according gradient.

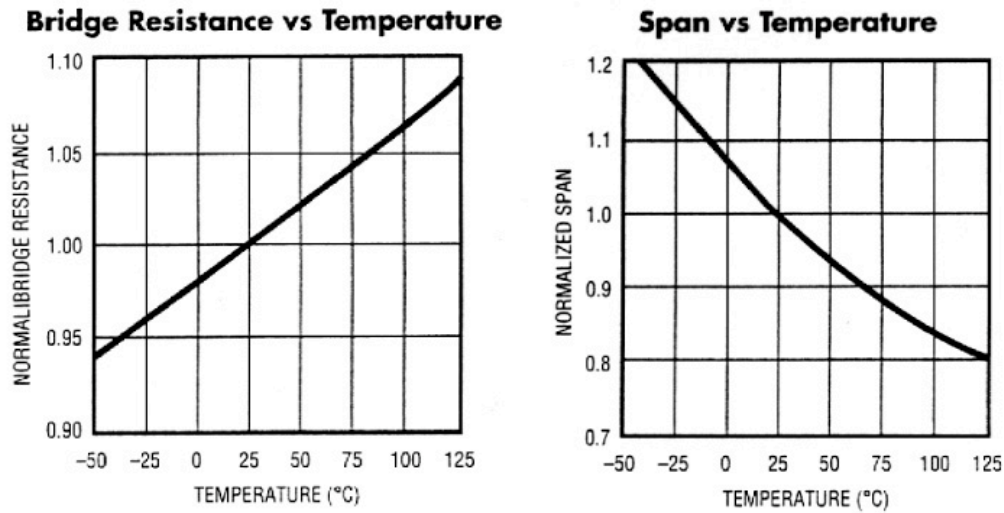


Figure 16: SenSym SX-series bridge resistance and span vs. temperature [27]

Around 10 years ago, it was common to use thermistors to vary the excitation current with temperature. Nowadays it can be done more precisely with integrated circuits, namely the LM334. The LM334 is a programmable constant current source with an output current that rises linearly with temperature at $+0.336\%/^{\circ}\text{C}$. From the Span vs. Temperature graph for the SX15GD2 in Figure 16, a linear approximation to the slightly curved line segment between 0°C and 70°C can be made. Using the slope of this segment, resistor values can be chosen to "program" the LM334 such that the pressure transducer will be accurate over this range.

In an open-water environment, water temperatures and conditions can vary over a large range. This was first introduced back in Chapter 2 when discussing the thermal profile of water. As temperature can vary sharply with depth, compensation circuitry of the depth transducer is critical in ensuring accurate results. As such, the LM334-based compensation method has been adopted for the AUV *Mako*. It is quoted as being able to provide temperature compensation with an accuracy of $<1\%$ [26].

3.4 Compensation and Amplification Circuit

The circuit in Figure 17 was chosen to both temperature-compensate and to amplify the 110mV span of the SX15GD2 pressure transducer to a 0-4.9V linear output capable of being directly interfaced with *Mako's* EyeBot controller. This circuit is

used, however that would limit the accurate range of operation of the depth sensor to $25 \pm 15^\circ\text{C}$ at around $\pm 2\%$ accuracy [27].

The final two regions, yellow (labelled 3) and green (labelled 4), provide common-mode-rejection and the final stage of amplification in order to scale the signal to the desired output span of 0-4.9V. This span of 0-4.9V corresponds to the range of the EyeBot's 10-bit analogue to digital converter (ADC). The resistors R_5 and R_p determine the output range of the circuit. For a 0-4.9V output, R_5 was chosen as $1.82\text{k}\Omega$ and R_p as a $5\text{k}\Omega$ potentiometer for fine adjustment. These values were determined from Table 3 given in the SenSym SX-series datasheet [27].

Again, in the yellow region (labelled 3), precision LT1014 amplifiers were chosen for temperature stability and overall linearity. However, in the green region (labelled 4), the LM10CN precision reference and operational amplifier was chosen. The leftmost op amp in the green region (labelled 4) has an internal 200mV precision voltage reference at its unconnected inverting (+) input. This provides a precision reference, V_R , to which the output signal will be relative.

3.5 Fabrication and Calibration

3.5.1 Fabrication

During May and June of 2005, Jonathan Brant from the UWA Department of Electrical, Electronic & Computer Engineering's Electronics Workshop, fabricated the depth pressure sensor. A picture of the completed sensor is shown in Figure 18.

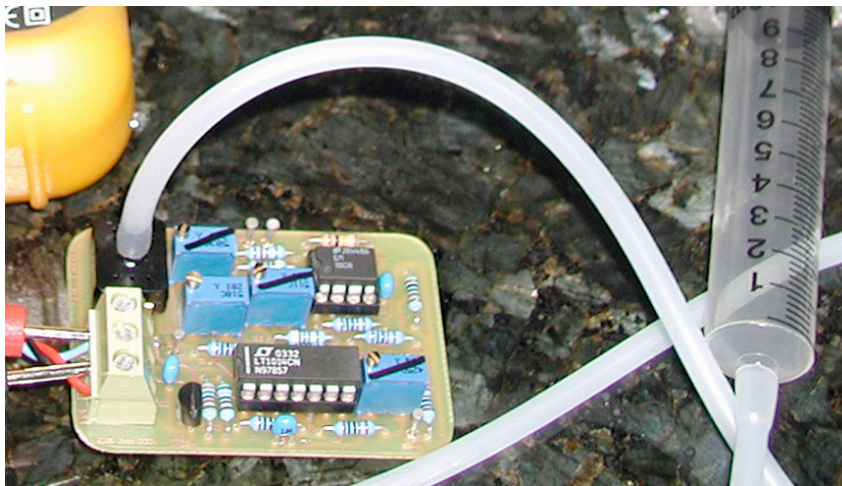


Figure 18: Fabricated depth pressure sensor PCB

3.5.2 Calibration

Using a syringe (visible in Figure 18) the sensor is calibrated via the four blue potentiometers. In Figure 18, three of the four have black lines across them. These three are for adjusting the common mode rejection ratio (CMRR), offset voltage (V_{offset}) and the reference voltage (V_R) of the amplifier respectively. The final potentiometer that is unmarked is for adjusting the span of the output voltage. With this potentiometer, the sensitivity of the pressure sensor can be changed. That is, the output span can be changed from 0-4.9V to 0-10V, giving the pressure sensor a more accurate output over half its maximum pressure when sampled by the 0-4.9V EyeBot.

For calibrating the amplifier board, a procedure applies for setting the four potentiometers. Referring to Figure 17 the following procedure applies [27]:

1. **Setting the Common Mode Rejection Ratio**
 - a. Short the points A and B together
 - b. Place a digital multimeter between V_X and V_R and adjust the CMMR potentiometer until the voltage is 0.000V
2. **Setting the Offset Voltage**
 - a. Remove the short from A and B
 - b. Adjust the V_{OS} potentiometer until the digital multimeter between V_X and V_R again reads 0.000V
3. **Setting the Output Reference Voltage**
 - a. Adjust the output reference V_R potentiometer until the output voltage, V_O , is equal to 1.00V
4. **Setting the Output Span**
 - a. Use a syringe to apply full-scale pressure to the sensor. That is, for the SX15GD2, the volume of air must be halved. This would require pushing the syringe plunger from rest at 10cc in until it reaches 5cc
 - b. Adjust the output span potentiometer, R_P , until the output voltage is the desired maximum. E.g. 4.9V for 0-10m, or 10V if the AUV will remain above 5 meters

Note that the first three potentiometers, after initial calibration, should never need changing. If the fourth output span potentiometer is changed to increase or decrease

the maximum depth or sensitivity of the pressure sensor, then the API (detailed in Appendix A) must be updated in order to properly translate the 10-bit ADC reading to an appropriate AUV depth in millimetres.

3.6 Mechanical Design

Chapter 2 introduced Hydrostatic Pressure, Pascal's Law and Boyle's Law. These concepts are used in this section to explain the mechanical design of the depth pressure sensor. Below in Figure 19 is a diagram of the mechanical design of the waterproof circuit board enclosure.

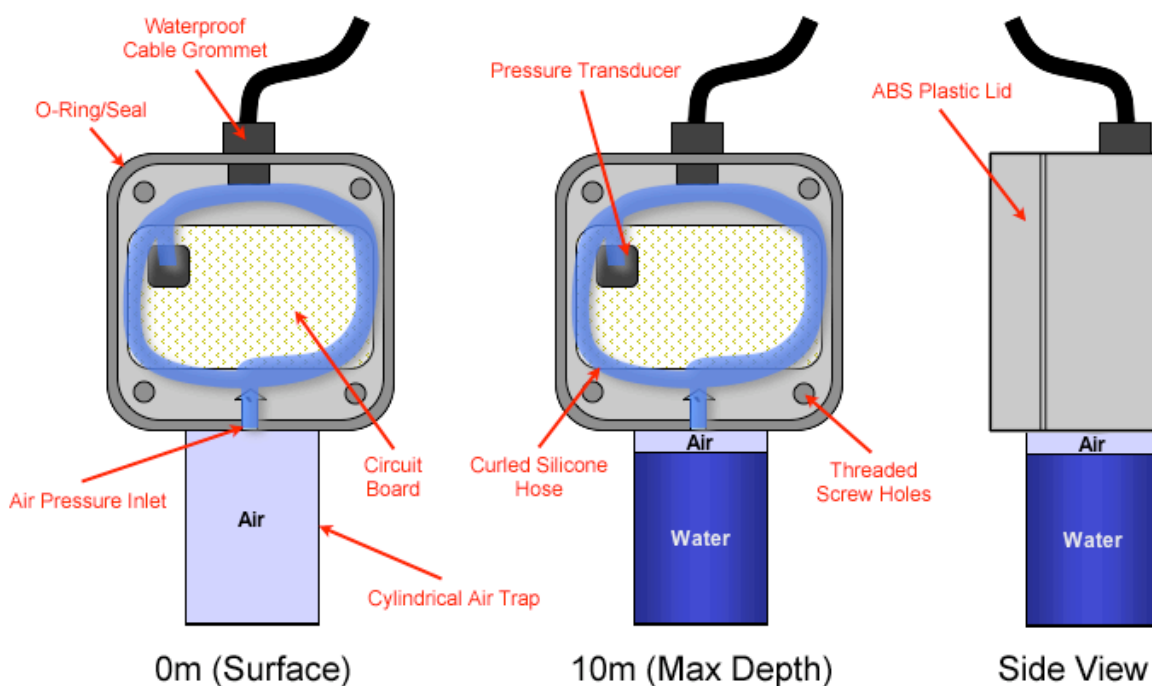


Figure 19: Depth pressure sensor - mechanical design

Once calibrated, the circuit board in Figure 18 was mounted inside the square waterproof ABS plastic enclosure shown in Figure 20. A waterproof plastic grommet was used to secure the four-core cable carrying the 12V power supply and the output signal from the pressure sensor amplifier. High pressure, very flexible, silicone model-car fuel hose is used to trap air between the pressure transducer and the surrounding water. Because water will damage the pressure sensor if it reaches the internal Wheatstone Bridge, fifty centimetres of hose is curled five times inside the enclosure. This clever technique used by Alec Duncan at Curtin University of

Technology means that any water inside the hose would simply sit in the bottom of the loops.

Taking this idea one step further, the cylindrical air trap was added. From Boyle's Law, when the pressure sensor reaches 10m deep (specification maximum) the volume of trapped air will have halved. Without the cylindrical air trap, at this depth water would be reaching 2.5 turns into the hose. Any water left sitting in the bottom of the curls after surfacing could evaporate and later condense inside the pressure transducer damaging it. For this reason, the cylindrical air trap was chosen to be slightly greater in volume to the air trapped in the hose. Thus at the maximum rating of the depth sensor the water will still not (but almost) reach the curled hose.

The curled hose is firmly attached at the inlet via a barbed fuel hose fitting and a cable tie. Expansion of the fuel hose was considered. However, as the trapped air pressure changes to match the hydrostatic force exerted the water, it will not lead to any inaccuracies.

3.7 Mounting the Depth Pressure Sensor on Mako

The finished pressure sensor was glued to the end of *Mako's* lower hull. Glue was used rather than screws as screws can lead to the hull leaking if they are loosened by knocks and bumps. The hollow upper hull and heavy loaded lower hull prevent roll. Thus mounting the pressure sensor in this location means that the curls are in a direction that the AUV *Mako* doesn't naturally move. This will restrict the movement of water through the curls to the sensitive pressure transducer. A photo of the mounted depth sensor is shown in Figure 20.

The cable for the depth sensor is secured through the hull using epoxy resin and a threaded bung. The relevant wires were spliced into the DB-25 tray connector so that they connect painlessly when sliding in the electronics tray. The output of the pressure sensor is currently connected to the sixth input of the AUV's EyeBot controller via a 4.7V zener diode acting as a voltage clamp. The 4.7V zener diode will prevent damage to the EyeBot's analogue to digital converter (ADC) in the event that

a voltage higher than 4.7V is reached on the pressure sensor output by bad calibration or otherwise.



Figure 20: Installed depth sensor

Chapter 4

Sonar Multiplexing System Design

This chapter will detail the methodologies behind the design of the sonar multiplexing system, building on the theory and background information contained in Chapter 2.

4.1 Importance of Sonar

An active sonar system is important for three main reasons:

- It provides obstacle and collision avoidance. The AUV *Mako* is programmed to stop if it believes it's about to collide with an obstacle such as a wall.
- The sonar system will allow *Mako* to perform tasks such as "wall following".
- When combined with the other sensors, it should be possible to use sonar data to calculate the placement of *Mako* within the pool.

Ionik Consulting is an engineering company specialising in the protection of pipelines and other assets in the exploration and production industries. They were the successful tenderer for the recent Total Indonesia Pipeline Management Services (PIMS) contract. Earlier this year, a UWA graduate and representative of Ionik Consulting described that in a realistic under-sea environment, sonar is often used to avoid obstacles in Remotely Operated Vehicles (ROVs) when the visibility is too low to navigate using the cameras.

4.2 +Design Requirements and Aims

Prior to the commencement of this project, the AUV *Mako* had two sonar transducers (one facing forward and one facing down) and one sonar controller that could be manually connected to either of these two transducers. The aim of this section of the project is to install new port (left) and starboard (right) facing transducers and to develop a multiplexing system to interface all of these sensors to the EyeBot controller.

Minh Nguyen in his 2004 thesis entitled *Design of an Active Acoustic Sensor System for an Autonomous Underwater Vehicle* identified the following four shortcomings of using the Navman Depth 2100 as an AUV sonar system [18]:

- an inaccurate resolution of 10cm;
- a slow data rate of 1Hz;
- serial interface; and,
- a lack of programmability

The sonar multiplexing system described in this chapter can directly address two of these problems, the serial interface and the lack of programmability.

The serial interface is a problem because of the limited number of serial ports available on the EyeBot controller. As it stands, four transducers would require four controllers, each requiring a separate serial port to interface it with the EyeBot. Using the property that each Navman Depth 2100 controller only outputs a temporally small amount of text NMEA 0183 data, the first aim of this design will be to concatenate the NMEA data from multiple Navman Depth 2100 controllers onto one RS-232C serial line for the EyeBot.

It was theoretically determined and experimentally justified that two Navman Depth 2100 transducers pointing in the same or diametrically opposite directions will interfere with each other due to reflections. This will cause erratic readings on both of the Navman 2100 controllers. This concept is illustrated in Figure 21. If the leftmost transducer sends out a ping, the rightmost transducer will also receive this ping resulting in erroneous measurements.

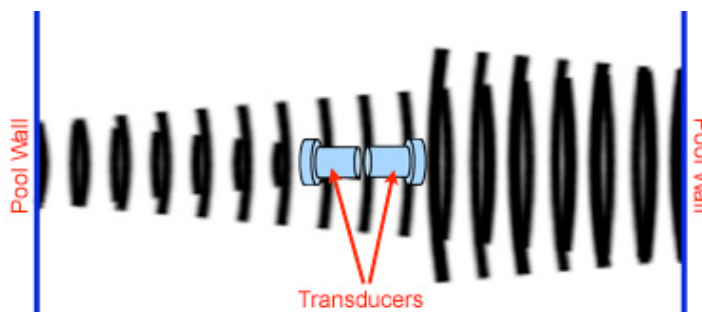


Figure 21: Opposing transducers will interfere

However, it was experimentally verified that transducers perpendicular to each other pose no problem in most cases. This result means that only two expensive Navman

Depth 2100 controllers are required to drive the four transducers on the AUV as only the perpendicular transducers can operate simultaneously. This forms the second aspect of the sonar multiplexing system design - transducer multiplexing. An overview of the overall sonar multiplexing system can be seen below in Figure 22.

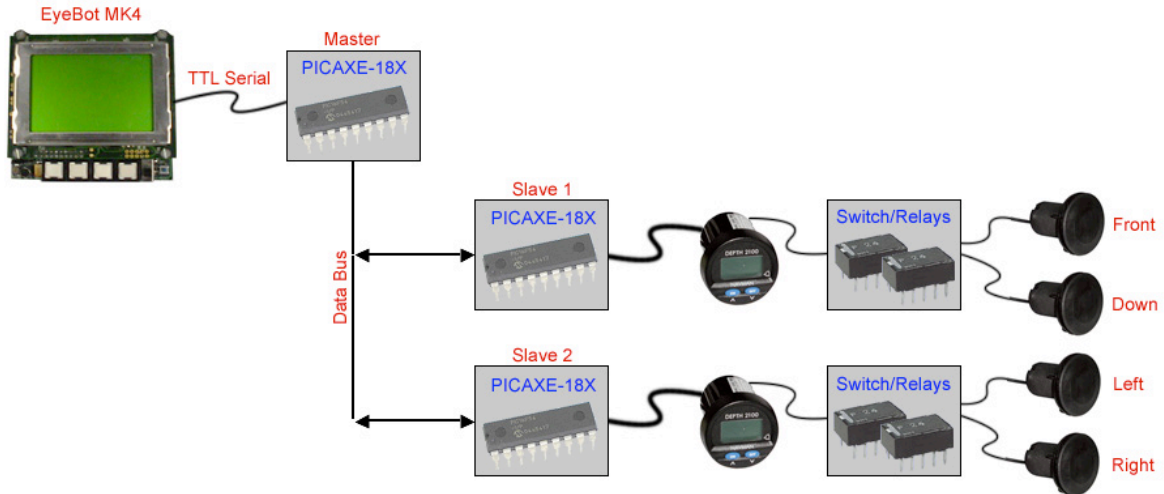


Figure 22: Sonar multiplexing system - overview

4.3 Controller NMEA 0183 Multiplexing

As the sampling rate of the Navman Depth 2100 controllers is already slow, in order not to increase it further, two independent buffers are used to receive and hold the serial NMEA 0183 data from each controller. Temporarily storing the data in independent buffers means that it can be accessed or relayed on request from the EyeBot rather than the EyeBot waiting up to one second for the next transmission from the controllers. This also avoids the situation where data is lost due to both Navman Depth 2100 controllers attempting to transmit at the same time over one serial line.

Commercial NMEA 0183 multiplexers are available however these units are unjustifiably expensive and would be difficult to use in this situation as the two Navman Depth 2100 controllers send out indistinguishable NMEA messages. This section will cover the design of a customisable NMEA multiplexer, using three PICAXE microcontrollers.

4.3.1 PICAXE-18X Microcontroller

PICAXE microcontrollers are essentially regular PIC microcontrollers. However, they're loaded with a special bootstrap program that allows them to run simple programs written in PICAXE BASIC. Several different types are available, and Figure 23 shows an overview of their features.

PICAXE Type	IC Size	Memory (lines)	I/O Pins	Outputs	Inputs	ADC (L =low)	Data Memory	Polled Interrupt
PICAXE-08	8	40	5	1-4	1-4	1L	128 - prog	-
PICAXE-08M	8	80	5	1-4	1-4	3	256 - prog	Yes
PICAXE-18	18	40	13	8	5	3L	128 - prog	-
PICAXE-18A	18	80	13	8	5	3	256	Yes
PICAXE-18X	18	600	14	9	5	3	256 + i2c	Yes
PICAXE-28A	28	80	20	8	8	4	64 + 256	Yes
PICAXE-28X	28	600	21	9-17	0-12	0-4	128 + i2c	Yes
PICAXE-40X	40	600	32	9-17	8-20	3-7	128 + i2c	Yes

Figure 23: PICAXE product comparison [20]

For the design of the sonar NMEA multiplexer, the PICAXE-18X was selected. Two of these microcontrollers will be used as the buffers to receive and hold the data from the two Navman Depth 2100 controllers, while a third will provide the interface between the EyeBot and the buffers. This master-slave type relationship is shown in Figure 22. The PICAXE-18X was chosen, as it is the most cost-effective PICAXE supporting the NMEA 0183 baud rate of 9600bps, used by the Navman Depth 2100 controllers.

4.3.2 TTL/CMOS and RS-232

As described in Chapter 2, NMEA 0183 uses what is essentially an RS-232C serial interface to transfer the text "sentences" at $\pm 15V$ logic levels. These high $\pm 15V$ logic levels preclude the possibility of directly connecting the NMEA 0183 lines of the Navman Depth 2100 controllers to the PICAXE microcontrollers. As PICAXE microcontrollers operate at TTL/CMOS voltage levels of 0V and +5V, external circuitry must be used to transpose to and from RS-232C $\pm 15V$ logic levels.

4.3.2.1 Simple RS-232C TTL conversion

For receiving RS-232C data on a TTL device, a simple "voltage divider" [20] can be used to lower the voltage levels from $\pm 15\text{V}$ to 0V and $+5\text{V}$. Likewise, as the logical 1 decision boundary for RS-232C is around $+3$ volts, often sending a $+5\text{V}$ TTL signal to an RS-232C receiver will work perfectly provided that the receiver assumes 0V (or lower than $+3\text{V}$) is logical 0. This technique is a cost effective solution to the problem of level conversion and is utilised on the non-frequently used programming ports of the PICAXE microcontrollers for the sonar multiplexing board. A circuit diagram of the resistive voltage divider used is shown in Figure 24 where "TX" stands for transmitter and "RX" stands for receiver.

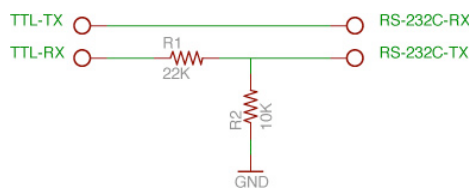


Figure 24: Simple RS-232C to TTL conversion

4.3.2.2 Accurate RS-232C TTL conversion

When attempting to use the simple method of RS-232C to TTL conversion, the PICAXE microcontrollers were unable to accurately read the NMEA data from the Navman Depth 2100 controllers. The first byte (8 bits) was being received correctly. However, after that, the remainder of the NMEA sentences were being corrupted. Ivan Neubronner, the resident PICAXE expert at UWA, recommended using a "MAX232" integrated circuit to accurately transpose the NMEA 0183 RS-232C $\pm 15\text{V}$ voltage levels to TTL 0V and $+5\text{V}$ levels for the PICAXE. This provided an effective and simple solution to the problem and was used in the final sonar multiplexing system design. It is suspected that the RS-232C signal output from the Navman Depth 2100 controllers is rather flaky and is corrected by the MAX232 integrated circuit while being converted to TTL level. Only one MAX232 was required to interface the two Navman Depth 2100 controllers to the two slaves as each MAX232 contains two RS-232C to TTL level converters.

4.3.3 Master and Slave Configuration

Now it has been established how the slave PICAXE microcontrollers receive the NMEA 0183 data from the Navman Depth 2100 controllers, the remaining problem is

how this data is sent to the EyeBot. The process follows that when the new EyeBot C++ function:

```
int CSonar::GetDistances(float *dist1, float *dist2);
```

is called inside a program, the EyeBot contacts the master PICAXE on the sonar multiplexing board. The master sends a signal to each of the slaves to return the last data they received from the Navman controllers. Once received from the slaves, the master then returns this data to the EyeBot and the function call is complete. Due to the buffering by the slaves, this process is faster than calling the previous three functions twice

```
int CEcho::ObtainMessage();  
int CEcho::MsgCheck();  
int CEcho::ObtainDistance(float *dist);
```

to receive the current distances from Minh Nguyen's API [18].

4.4 Transducer Multiplexing

As mentioned previously, because only perpendicular transducers can operate simultaneously, two Navman Depth 2100 controllers can be used to operate all four transducers. Evident in Figure 22, this means Navman "Controller 1" must be switched between the front and down transducers, and "Controller 2" must be switched between the left and right transducers.

Double-pole-double-throw, 240V AC, 30W, Telecom relays were selected for this transducer switching. Requiring 12V and 12mA to switch, these were mainly selected because they're small (14x5x9mm) and because they have a high dielectric strength of 1000V AC between the open contacts and the coil. As the ping pulse of the Navman Depth 2100 controllers is significantly high in voltage, the high dielectric strength prevents sparking and crosstalk between the controller and the transducers. A photo of the miniature Telecom relays is shown in Figure 25 below.



Figure 25: Telecom relays

One relay is used per transducer giving fully customisable "make before break" or "break before make" characteristics. The respective slave PICAXE microcontrollers control the four relays. The switching process occurs by the EyeBot contacting the master and communicating the details of the switch. The master then contacts the involved slave PICAXE microcontrollers and waits for confirmation that the switch has occurred. When the switch has occurred, the master returns a successful signal to the EyeBot that is forwarded to the user program. Switching and querying is done via the following EyeBot C++ functional prototypes:

```
/*
 * Select the two transducers for controller1 and controller2.
 *
 * char controller1 can be:
 *   'f' (front), 'd' (down), 'n' (none) or null (leave it unchanged)
 * char controller2 can be:
 *   'l' (left), 'r' (right), 'n' (none) or null (leave it unchanged)
 *
 * Returns 1 on success
 */
int CSonar::SelectTranducers(char controller1, char controller2);

/*
 * Gets which transducers are currently connected.
 *
 * char controller1 can be:
 *   'f' (front), 'd' (down), 'n' (none) or null (leave it unchanged)
 * char controller2 can be:
 *   'l' (left), 'r' (right), 'n' (none) or null (leave it unchanged)
 *
 * Returns 1 on success
 */
int CSonar::CurrentTranducers(char *controller1, char *controller2);
```

4.5 Final Design, Construction and API

Appendix B shows a full-page schematic diagram of the final design of the sonar multiplexing system. Jonathan Brant from the UWA Electrical and Electronics Engineering Electronics Workshop fabricated this schematic diagram. A photo of the final circuit board it shown below in Figure 26. The new sonar API is also documented in Appendix C.

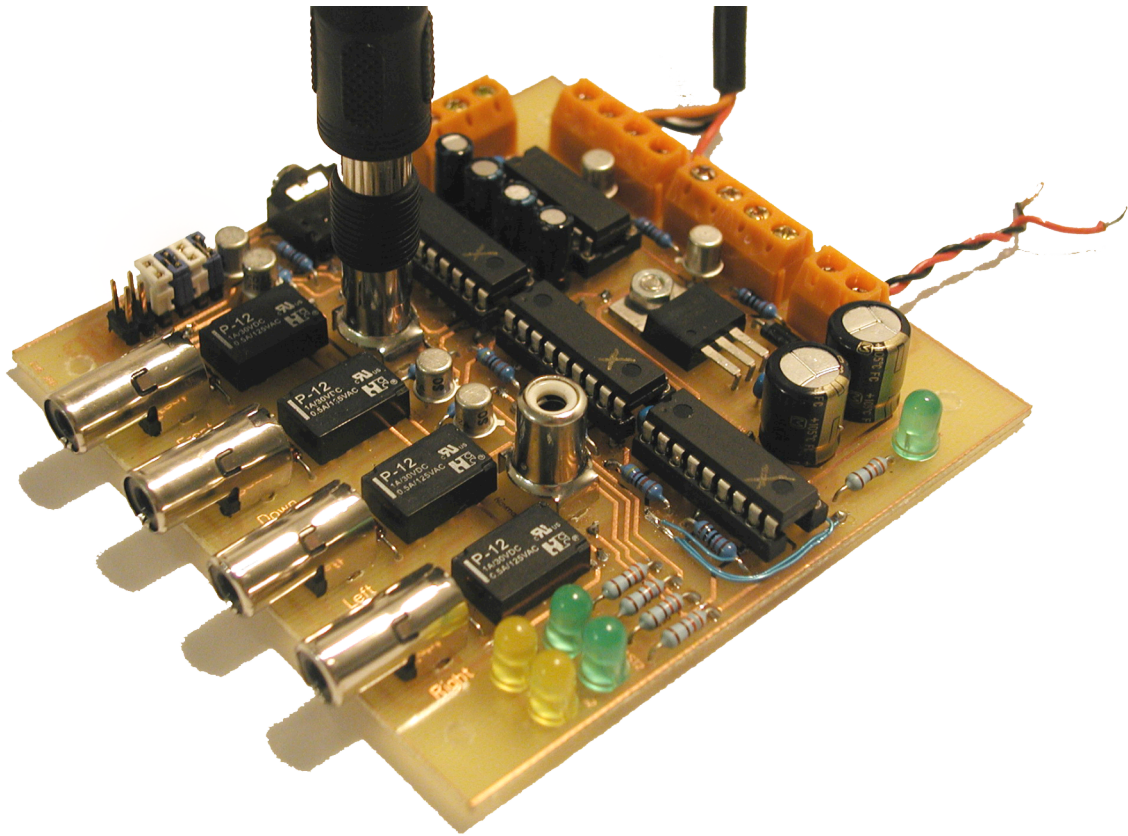


Figure 26: Fabricated sonar multiplexing system circuit board

Chapter 5

Experimental Procedures and Results

The three experiments performed on the depth sensor will be detailed in this chapter, followed by the three experiments performed on the sonar multiplexing system.

5.1 Depth Pressure Sensor

This section will detail the three experiments conducted on the completed depth pressure sensor. The first experiment is testing the output linearity, followed by an experiment addressing the electromagnetic interference (EMI) problems with the depth pressure sensor. The final experiment is to calibrate the depth pressure sensor application program interface (API).

5.1.1 Experiment 1: Output Linearity

5.1.1.1 Aim

The aim of this experiment is to test the linearity of the depth pressure sensor and amplifier by simulating a linear increase in pressure.

5.1.1.2 Background

As described previously, the pressure sensor and amplifier combination was selected for its overall output linearity.

5.1.1.3 Method

A syringe with a valve was connected to the pressure sensor input port. Every time the syringe plunger was pushed in by one notch, five recordings of the depth sensor output voltage were taken. A program written for the EyeBot automatically collects the five samples when the "Clock" button on the infrared remote is pushed. The data is sent out over Bluetooth to the computer recording the results.

Using the volume of the silicone hose, volume of the syringe and current atmospheric pressure, the simulated depth was calculated according to the equation:

$$p_1V_1 = p_2V_2 \quad (\text{Boyle's Law})$$

Where,

$$p_1 = 101.3kPa$$

$$V_1 = 1.04 \times \pi(0.004)^2 + 10 \times 10^{-6} m^3$$

$$= 6.228 \times 10^{-5} m^3$$

$$p_2 = \rho gh + p_{atmospheric} = d \times 9.8 + 101.325kPa \quad (\text{Hydrostatic Pressure})$$

$$V_2 = 1.04 \times \pi(0.004)^2 + \frac{i}{50} \times 10^{-5} m^3$$

and i is the syringe notch number (0 to 50) and d is the depth in meters below sea level.

5.1.1.4 Results

Solving these equations for each syringe notch and plotting it against the average output voltage yields the graph shown in Figure 27.

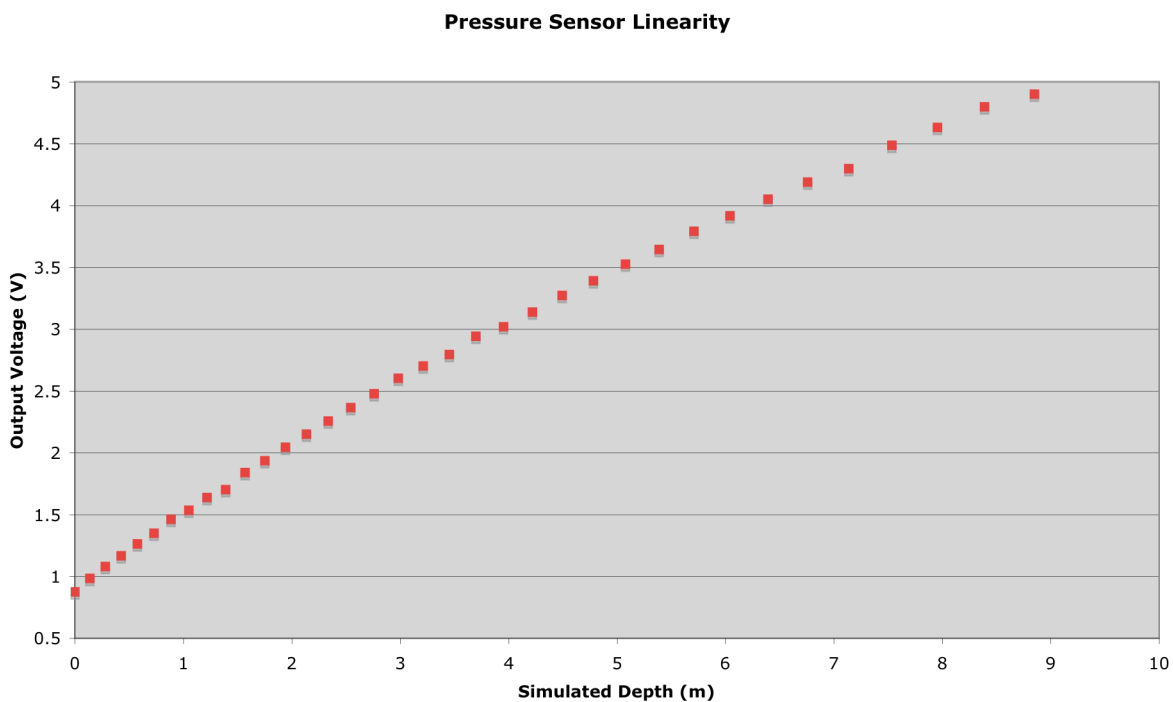


Figure 27: Simulated pressure sensor linearity

5.1.1.5 Analysis

The points in Figure 27 should form a straight line. It is quite close over the simulated range of 0 to 5m, however after that it appears to gradually flatten out. There are a number of possible reasons that could explain this non-linearity:

- Non-linearity of the pressure sensor and amplifier

- Expansion of the hose at pressures above the simulated 4 or 5 meters depth
- Air leakage at the syringe, hose or valve

Out of these possible reasons, the most significant air leakage from the syringe. When the assembly is submersed in water, at the higher pressures, air bubbles can be seen slowly escaping around the plunger. Hence the plot above is linear from 0 to 5 metres. However, after that air begins escaping from the syringe and causing the pressure to decrease.

When the AUV is operating in the water, the air pressure trapped in the sensor changes such that it is equal to the surrounding hydrostatic pressure. Thus, the changing volume of the hose through expansion and any small leakage of air from the AUV rolling slightly etc. will not affect the pressure reading. This is not the case for the syringe test as directly working with the volume of the air in order to change the pressure means that the pressure-volume product (Boyle's Law) must remain constant with no changes in volume from leakages or hose expansion.

5.1.2 Experiment 2: Noise and Electromagnetic Interference (EMI)

5.1.2.1 Aim

To test the effects of electromagnetic interference and supply voltage noise generated by the high current pulse-width modulated (PWM) motor drives on the sensitive pressure sensor amplifier.

5.1.2.2 Background

Electromagnetic interference is a major problem in most electronic devices where high currents and/or high frequency current fluctuations are present near sensitive analogue electronics. Other universities around the world designing AUVs have had serious problems with supply voltage noise and EMI due to pulse-width modulation (PWM) being used to vary the speed of the high-current motors. This was discovered to also be a problem for *Mako* soon after the installation of the depth sensor.

Pulse-width modulation (PWM) is the most commonly used method for controlling the speed of DC motors. It involves very rapidly (multiple times per second) turning on and off the voltage to the motor (in a variable square wave) in order to adjust the

power supplied to the motor. The problem of supply voltage noise occurs because for each fraction of a second that voltage is supplied to the motor, the motor draws a substantial current, causing the voltage of the 12V battery supply to fluctuate quickly. The second effect, EMI or unwanted induction, occurs because the rapidly fluctuating current in the power wires can result in current being induced in nearby signal wires. In an electromagnetic interference context, this unwanted exchange of energy is commonly known as "crosstalk" and can lead to substantial amounts of unwanted noise in signal and supply wires.

Pressure sensors are extremely sensitive and most have raw un-amplified output current spans in the vicinity of 100mA. Hence, any unwanted noise at the pressure sensor will be a major problem as it will be similar in magnitude to the legitimate sensor current.

5.1.2.3 Method

A program was written for the EyeBot controller that runs each motor at each possible forward and reverse speed for three seconds. During the three seconds at each speed, the air pressure is sampled every five-hundredths of a second, totalling sixty samples at each speed. The raw value from the EyeBot analogue to digital converter (ADC) was recorded and scaled to give a pressure in kilopascals. For this experiment the AUV was out of the water with the atmospheric pressure in the surrounding room (according to the pressure sensor) at approximately 97kPa.

This process was then repeated with the depth pressure sensor amplifier protected from the 12V supply voltage noise via the simple diode and capacitor circuit shown in Figure 28 below.

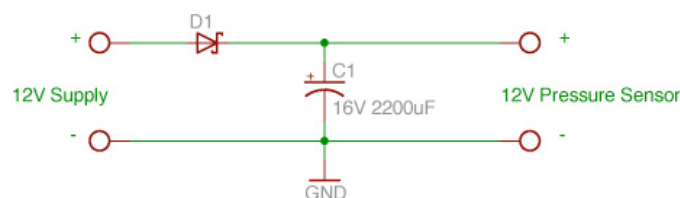


Figure 28: Fluctuation filtering circuit

The pressure sensor amplifier board is sensitive to supply voltage fluctuations and noise for two reasons. Firstly, the supply voltage is used to power the op amp that

provides the precision voltage that the pressure sensor is referenced to. The remainder of the circuit can amplify any fluctuations in this precision reference voltage. Secondly, the physical supply voltage traces on the pressure sensor amplifier circuit board are close to the sensitive signal traces. Noise from the supply voltage can be electromagnetically coupled (EMI) to the sensitive signal wires and be amplified by the circuit.

For these reasons, the noise and fluctuations of the power supply must be kept to a minimum via a circuit such as the one above in Figure 28. This circuit works because the capacitor, C1, essentially acts like a (small and fast) rechargeable battery. It stores the excess charge from when battery voltage is above 12V and quickly releases this charge when the voltage falls below 12V. Thus, the capacitor has the effect of smoothing the battery or supply voltage to 12V when the PWM motor drives are running. The diode, D1, acts like a one-way valve and stops the charge released by the capacitor from flowing back and being completely consumed by the PWM drive. With the diode, only the pressure sensor takes advantage of the smoothed 12V supply. The other 12V parts of the AUV are insensitive to noise and the fluctuating 12V supply, so the limited energy provided by the capacitor is best spent being used only by the pressure sensor.

The goal of this experiment is to show graphically the effects of this noise and electromagnetic interference (EMI) occurring from the PWM drive and to observe effects of the simple diode-capacitor noise filter.

5.1.2.4 Results

Using the data collected by the program, the standard deviation of the sixty pressure readings at each speed was calculated. Two of the graphs shown below are for the stern (Figure 29) and bow (Figure 30). These two will be presented because these two motors are used in conjunction with the depth pressure sensor to maintain a desired depth underwater. The stern motor is also in close proximity to the pressure sensor, while the bow motor is at the opposite end of the vehicle. The remainder of the motors will be presented in Appendix D, along with the reverse directions for the stern and bow motors.

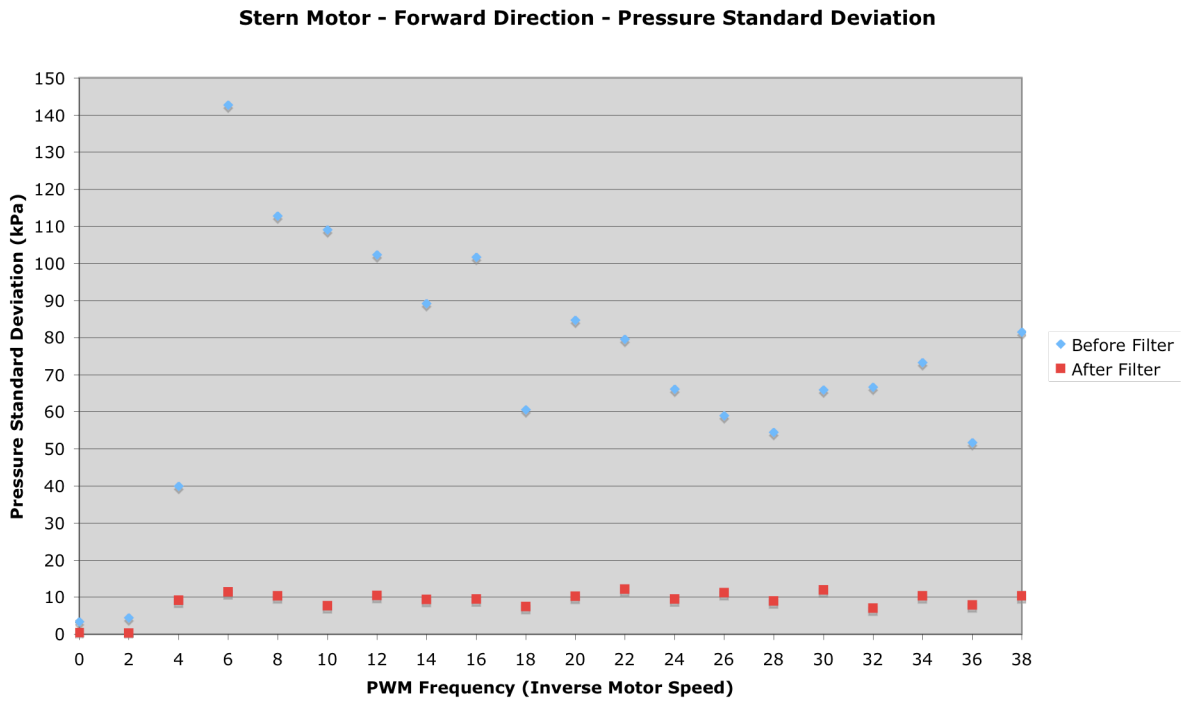


Figure 29: Stern motor, closest to the pressure sensor

Below in Figure 30 is the graph for the bow motor. The bow motor is the furthest from the pressure sensor.

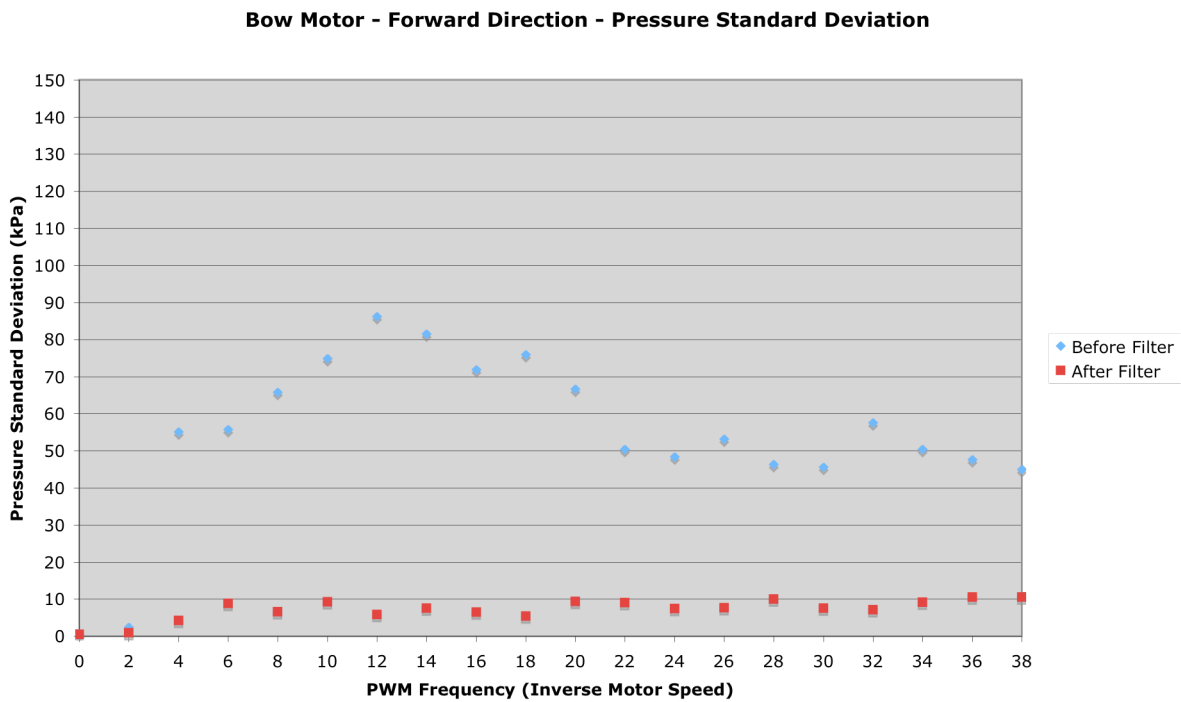


Figure 30: Bow motor, furthest from the pressure sensor

The two photos below in Figure 31 show the pressure sensor output waveform before and after the addition of the filtering circuit, for the same pressure.

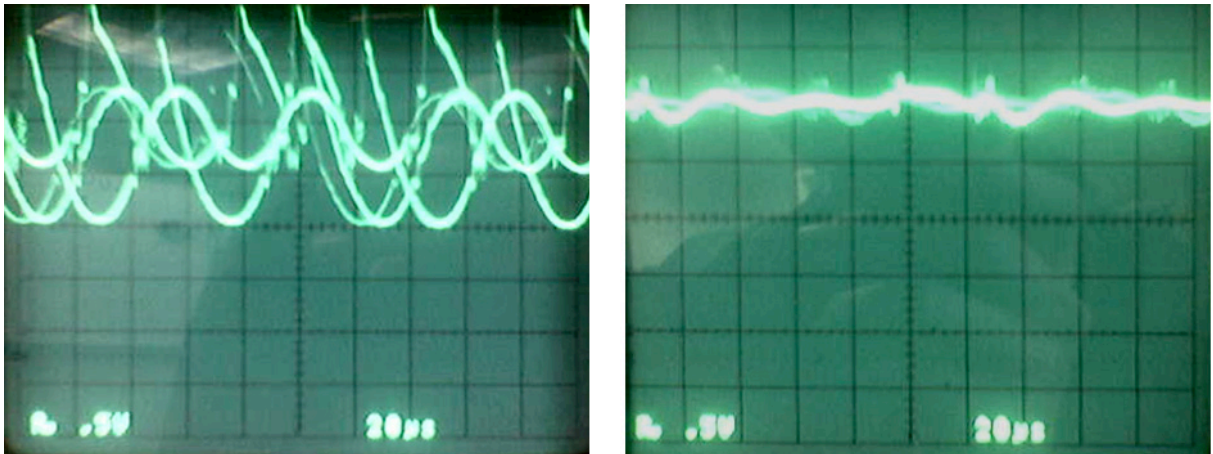


Figure 31: Pressure sensor output before (left) and after (right) the filtering circuit

5.1.2.5 Analysis

As mentioned in the method, the sensor recorded the surrounding pressure at the time of the experiment as 97kPa. Notice from the graph for the stern motor (Figure 29) that before the voltage fluctuation filtering circuit was introduced, the readings from the pressure sensor had a standard deviation of up to 142kPa – that is greater than the recorded surrounding pressure of 97kPa. Thus, without any protection, the supply voltage noise and fluctuations from the PWM drive renders the sensitive pressure sensor completely useless. Notice also that when the PWM drive frequency is at 0 (i.e. the motors are directly connected to the supply voltage and going full speed) the standard deviation before and after the protection circuit is similar and suitably low to enable accurate reading of the sensor. This is expected as the supply voltage is not rapidly fluctuating when the motors are directly connected because they will operate drawing a constant current.

From the graph for the bow motor (Figure 30), the standard deviation of the pressure before the filter was added is again too high to give a valid pressure reading. However, comparably it is lower than the stern motor (Figure 29). This could be the case for a number of reasons. Firstly, the thrust table in the motor API [29] reveals that more power needs to be supplied to the stern motor in order to make it operate at the same speed as the bow motor. Thus, greater voltage fluctuations will occur for the stern motor as it consumes more current for the same speed of operation.

Secondly, the fast moving magnetic fields created by the motor and the motor wires are further away from the pressure sensor for the bow motor. Thus, the direct effects of EMI may be less for the bow motor.

From the two oscilloscope screenshots shown in Figure 31, before the filtering circuit was added it is not surprising that pressure was indeterminate. After the filtering circuit was added, the output of the pressure sensor is seen to be much cleaner, except for some low amplitude noise. The depth sensor API (application program interface, detailed in Appendix A) removes most of this noise by taking three samples of the pressure and selecting the middle value.

5.1.3 Experiment 3: Depth Calibration

5.1.3.1 Aim

To calibrate the depth sensor API for pool water so that the depth (in millimetres) of the AUV can be accurately determined from the pressure sensor reading.

5.1.3.2 Background

From the background information chapter, determining the pressure at depth is described by:

$$p_{absolute} = \rho gh + p_{atmospheric} = d \times 9.8 + 101.325kPa \quad (\text{Hydrostatic Pressure})$$
$$p_{gauge} = \rho gh = d \times 9.8$$

This relationship relies on the atmospheric pressure being 101.325kPa and water having a density of 1000kgm⁻³. For salt or chlorine water (such as that in a swimming pool) the density ρ is not exactly 1000kgm⁻³, but more like 1030kgm⁻³.

5.1.3.3 Method

A tape measure and a rubber foot was attached to a two metre length of aluminium square hollow section in order to accurately lower the AUV in the water. This is shown in Figure 32.

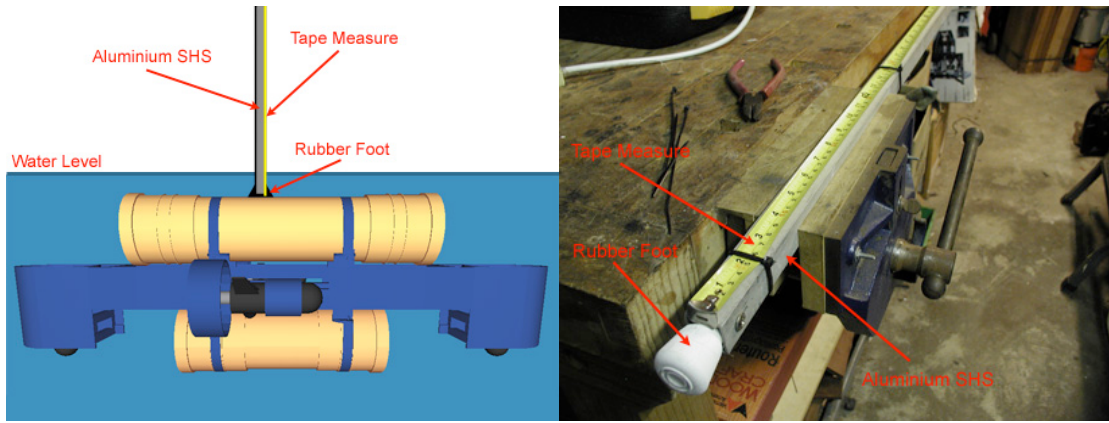


Figure 32: Measurement method and apparatus

Beginning with the AUV floating at the surface, the rubber foot was placed sitting on top of the AUV and the tape measure was adjusted to read 0mm. The aluminium length was used to push the AUV down in increments of 250mm. This is shown in Figure 32. At each increment, the analogue to digital converter (ADC) reading for the pressure sensor was recorded four times.

The distance from the bottom of the AUV to the rubber foot was measured and used to translate the depth measurements on the tape measure to the depth at the lowest point on the AUV. By using the lowest point on the AUV to reference the depth, it will be easy in the future to know whether the AUV will hit the bottom of the pool, given the depth of the water.

5.1.3.4 Results

The table below shows the results collected from this experiment:

Tape Depth	AUV Depth	1	2	3	4	Average
Atmospheric Reading		217	216	218	213	216
0	500	294	293	303	297	296.75
250	750	355	356	352	361	356
500	1000	413	417	415	407	413
750	1250	468	467	465	467	466.75
1000	1500	526	526	528	527	526.75
1250	1750	591	594	592	596	593.25

Using this data to plot the actual depth of the AUV against the pressure reading from the ADC gives Figure 33 below.

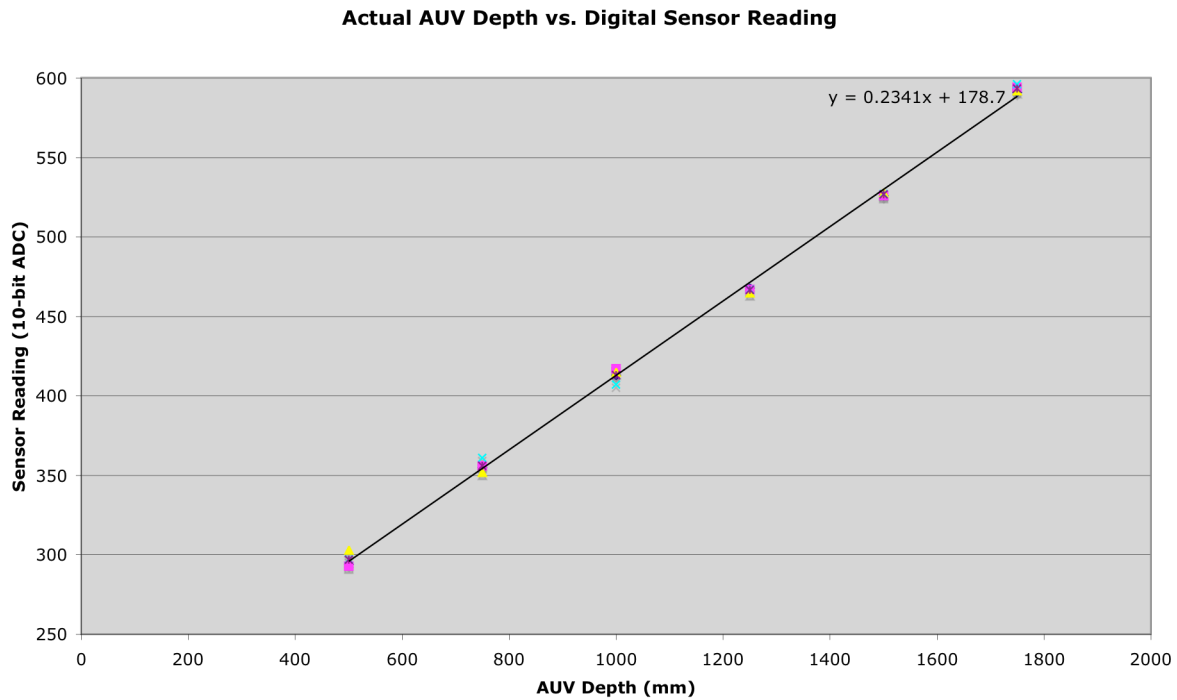


Figure 33: Actual AUV depth plotted against the pressure sensor reading

5.1.3.5 Analysis

The linear trendline for the results is displayed on the graph in Figure 33 above. The inverse of this equation is used in the depth sensor application program interface (API) to translate the pressure sensor reading into a depth in mm. The depth sensor API is available on the CD-ROM and outlined in Appendix A.

Notice the linearity of the readings; this again proves the linearity of the pressure sensor and amplifier.

5.2 Sonar Multiplexing System

This section will detail the four experiments conducted on the Navman Depth 2100 and sonar multiplexing system. The first experiment is testing the beam width and shadowing of the Navman Depth 2100 transducers. The second experiment tests two perpendicular transducers simultaneously. Finally two methods will be tested for wall following - a standard proportional controller and a Fuzzy Logic controller.

5.2.1 Experiment 1: Beam Width and Shadowing

5.2.1.1 Aim

The aim of this experiment was to make an estimate whether multiple transducers would operate simultaneously by measuring the beam width of the Navman Depth 2100 transducers.

5.2.1.2 Background

During this experiment, two of the three transducers owned by UWA were permanently mounted on the AUV, leaving only this one to test freely. With the purchase of another transducer, the remaining free transducer and the new one could be mounted on the AUV facing port (left) and starboard (right). The aim of this experiment was to better estimate whether another transducer should be purchased.

As shown previously in Figure 21, it is understood that transducers lying inside the beam path of other transducers will interfere. This experiment was designed to measure the beam width of the transducers in order to predict the minimum angle the transducers must be separated by in order to not interfere. If this angle were too close to 90° , having left and right transducers on the AUV wouldn't be feasible.

5.2.1.3 Method

A jig was developed to allow the angle of the transducer in the water to be accurately set. An obstacle was placed in the centre of the pool and the angle of the transducer was varied over 90° with the sonar distance measurements recorded every 1° . Photos of the experimental set-up are shown below in Figure 34.

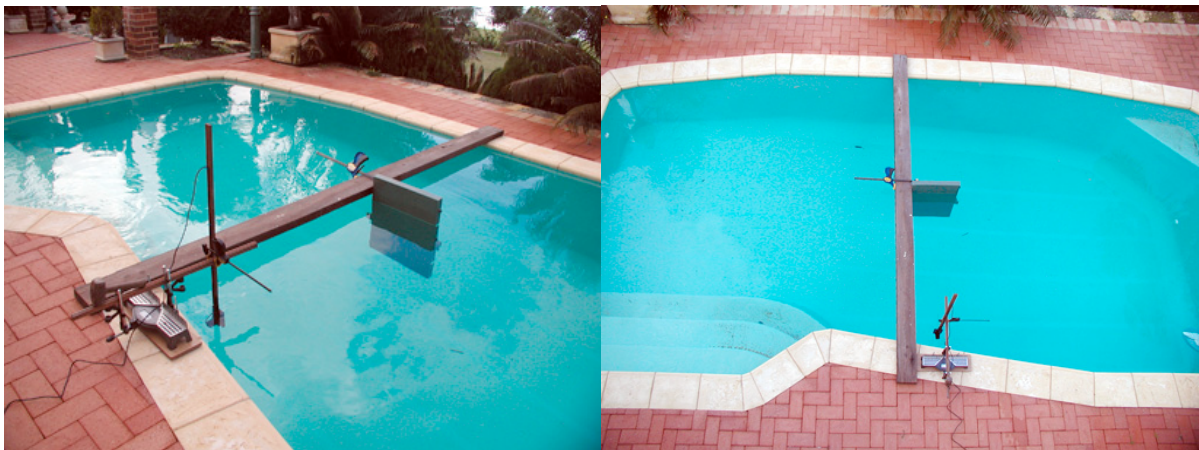


Figure 34: Beam width and shadowing set-up

5.2.1.4 Results

The results were converted from cylindrical polar to Cartesian coordinates and plotted using Excel. The graph below in Figure 35 shows the outline of the pool, the object and the mapping of the pool and object using the Navman Depth 2100.

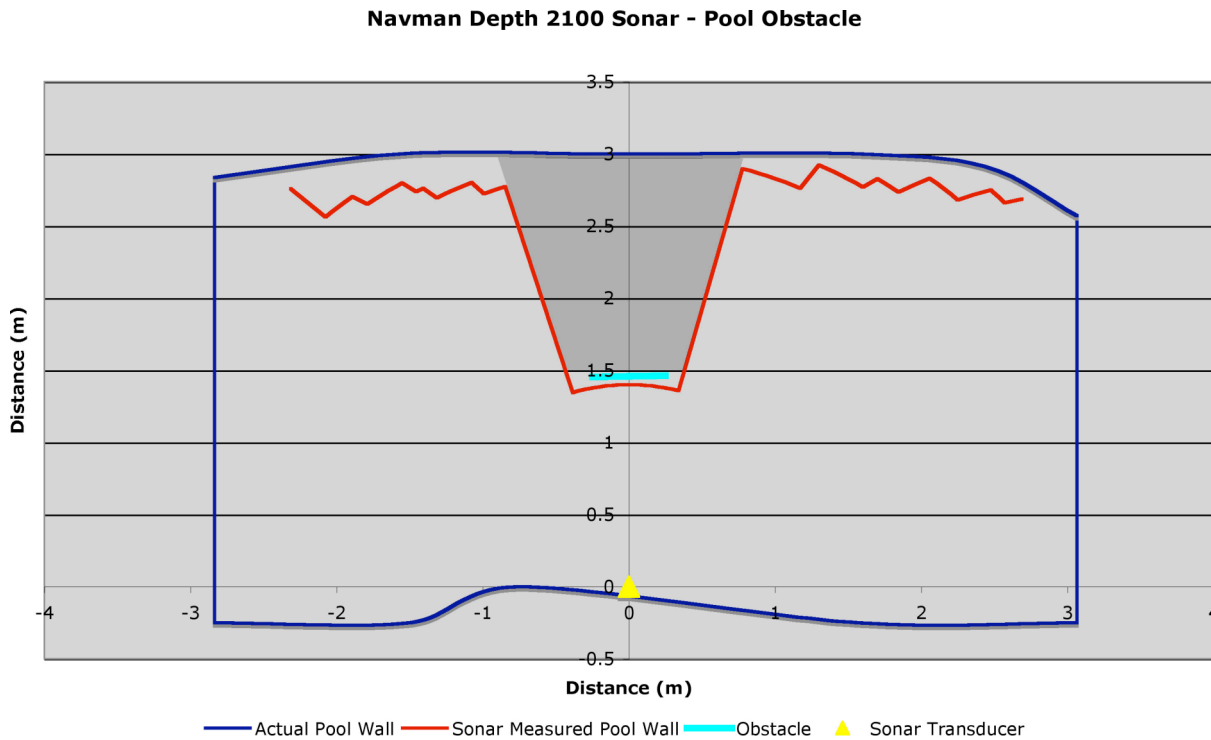


Figure 35: Mapping of an obstacle in the pool

5.2.1.5 Analysis

Comparing the bird's eye view of the pool set-up shown in Figure 34 with the sonar determined bird's eye view shown in Figure 35, the red jagged line in Figure 35 denotes the mapping made by the Navman Depth 2100.

The line is jagged due to the 10cm resolution of the Navman Depth 2100 controller. The red lines actually all form concentric circles, with 10cm between them, drawn around the sonar transducer. This is evident from the red semi-circle in front of the obstacle.

The darker grey area behind the obstacle is known as the shadow. This comes from the parallels that can be drawn between the ray nature of both light and sound. Similar to a person standing at the sonar transducer in the dark with a torch, objects within this shadow will not be seen by the torch or the sonar transducer.

The actual location of the pool wall does not perfectly match the average distance measured by the sonar system. This is due to two reasons. Firstly, the temperature and salinity of the water result in the speed of sound in the pool water being different from the seawater environment where the Navman Depth 2100 controllers are calibrated. Secondly, this difference is also likely to be due to inaccuracies in the timing method used by the Navman Depth 2100 controller.

By collapsing the flat obstacle into a point obstacle, the beam width of the Navman Depth 2100 transducers can be estimated. From the Excel spreadsheet recorded during the experiment, the Navman Depth 2100 transducer has to pass the obstacle by 5° before it measured the pool wall rather than the obstacle. Multiplying this by two in order to include the other edge gives the beam width of the Navman Depth 2100 transducers as approximately 10° . This compares well with the beam width of 15° reported widely by boating users on the Internet.

From this experiment, for the transducers not to interfere, they must be separated by a minimum angle of 10° .

5.2.2 Experiment 2: Perpendicular Transducers

5.2.2.1 Aim

To ensure that perpendicular transducers will in fact work properly without interference.

5.2.2.2 Background

After the success of Experiment 1 in proving the beam width of the transducers, the fourth transducer was purchased. This was the final short experiment to ensure that perpendicular transducers could operate together before permanently mounting the third (port) and fourth (starboard) transducers on AUV.

5.2.2.3 Method

The two free Navman Depth 2100 transducers were mounted on the ends of wooden lengths (similar to Figure 34) and tested in various locations around the pool to check for erroneous measurements due to interference.

5.2.2.4 Results

It was experimentally verified that perpendicular transducers would operate successfully. However, if a transducer was directly placed within the other transducer's beam width or reflected beam, erroneous measurements occurred.

5.2.2.5 Analysis

This result was as expected from Experiment 1. The design of the sonar multiplexing system went ahead on the outcomes of this final feasibility test.

5.2.3 Experiment 3: Wall Following – Proportional Controller

5.2.3.1 Aim

The aim of this experiment was to test the ability of the AUV to follow a wall to the left of the vehicle using a simple proportional controller.

5.2.3.2 Background

As introduced in Chapter 2, a wall following proportional controller works by:

- subtracting the current distance to the wall from the desired distance;
- multiplying the resulting difference by a gain constant K_p ; and,
- adjusting the motor speeds by this resulting difference gain product.

Hence, with a P controller, the further the AUV is away from the wall the sharper it will turn closer to the wall. Likewise, the closer the AUV is to the wall, the sharper it will turn away from the wall.

5.2.3.3 Method

A proportional control program with $K_p=10$ was written for the AUV and tested in the pool. The program was written to follow a wall to the left of the vehicle at a desired distance of one metre.

The distance from the wall was constantly sent out by the AUV over Bluetooth to a monitoring computer by the poolside.

5.2.3.4 Results

Videos of this wall-following experiment are available on the accompanying CD-ROM.

The plot below in Figure 36 shows wall-following using a proportional controller.

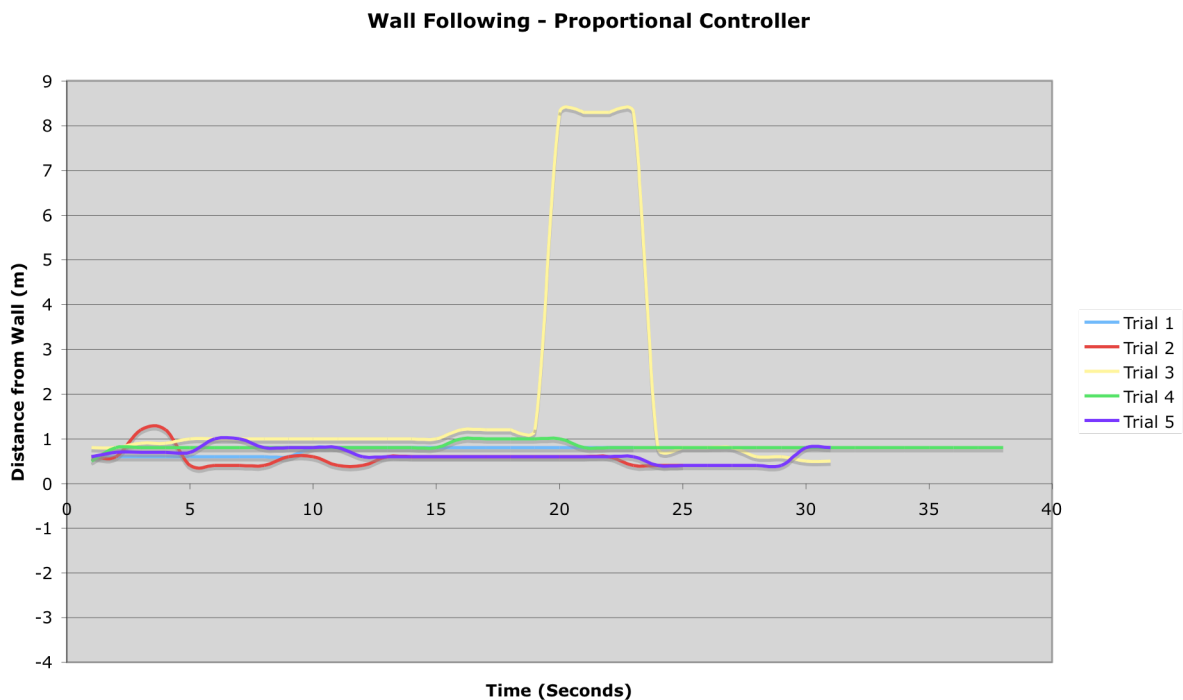


Figure 36: Wall-following using a proportional controller

5.2.3.5 Analysis

The first standout feature of the above plot, Figure 36, is the 8.3m peek at the 20-second mark. This is the problem of multipath detailed in Chapter 2. Occasionally the Navman Depth 2100 controller misreads the distance to the wall due to other multipath reflections returning with similar amplitude to the legitimate reflection.

Other than that, the AUV appears to stay at a regular distance from the wall. Some oscillations are visible at the beginning of the plot, but not of magnitude large enough for the AUV to lose the wall.

5.2.4 Experiment 4: Wall Following – Fuzzy Logic

5.2.4.1 Aim

To test a more sophisticated wall following algorithm, namely Fuzzy Logic, to compare the AUV's ability to follow a wall.

5.2.4.2 Background

Fuzzy Logic, as introduced in Chapter 2, is a more complex form of control that not only takes into account the current distance from the wall, but also the rate of change of the distance from the wall.

Generally formed from a series of linguistic rules, Fuzzy Logic is often used to control more complex and often non-linear systems. Common systems using Fuzzy Logic are ABS brakes, traction control systems, air conditioners and various home appliances such as washing machines. The Fuzzy Logic arrangement used in this situation will be described and explained in the method.

5.2.4.3 Method

A Fuzzy Logic controller was designed based on the following linguistic rules:

- IF too far from the wall AND getting closer THEN head towards the wall
- IF at the desired distance AND getting closer THEN head away from the wall
- IF too close to the wall AND getting closer THEN head away from the wall

- IF too far from the wall AND no change THEN head towards the wall
- IF at the desired distance AND no change THEN keep heading straight
- IF too close to the wall AND no change THEN head away from the wall

- IF too far from the wall AND getting further THEN head towards the wall
- IF at the desired distance AND getting further THEN head towards the wall
- IF too close to the wall AND getting further THEN head away from the wall

From these linguistic rules, the following membership functions were developed:

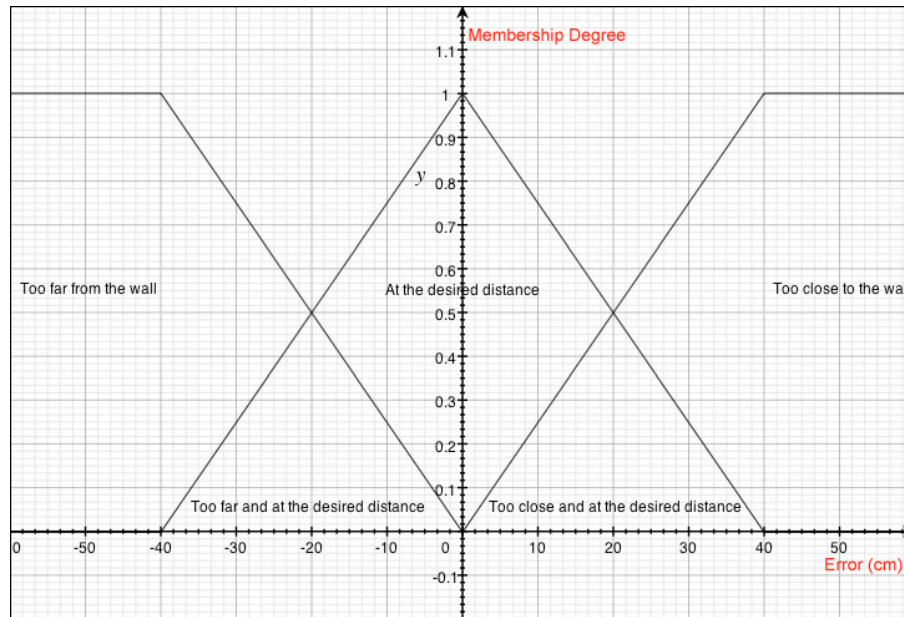


Figure 37: Error member function

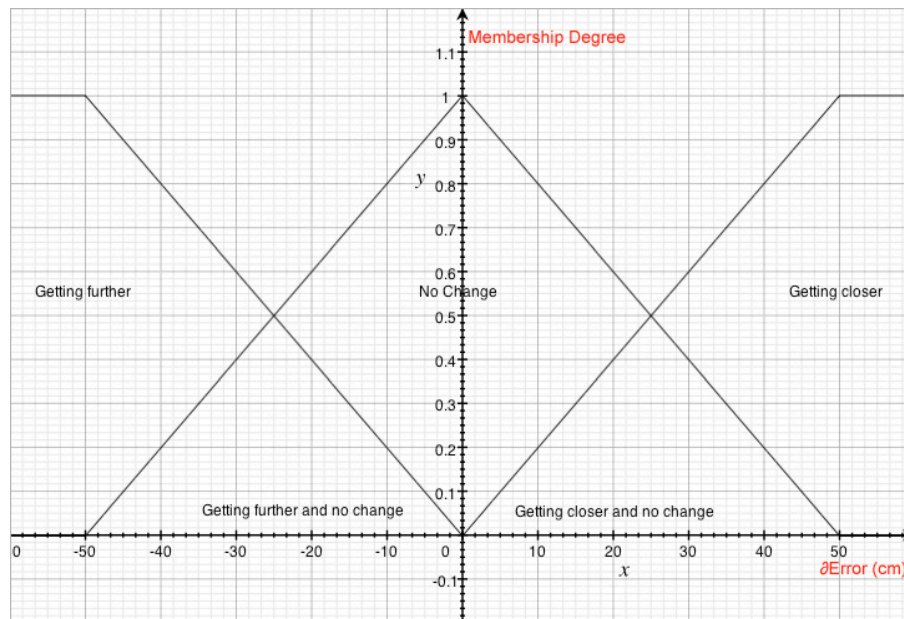


Figure 38: Error rate of change membership function

For each measurement taken, the error (desired minus actual distance) and error rate of change (previous error minus current error) are calculated and used to determine the membership to each of the functions above. For example, if the error is 10cm, from the error membership function above, the AUV will be travelling 0.25 "too close to the wall" and 0.75 "at the desired distance". Likewise, if the error rate of change is 20cm, the AUV will be travelling 0.4 "getting closer" and 0.6 "no change".

In a further process called "Output Combination", the root-sum-square of each of these memberships is taken. That is, from the linguistic rules, the total amount that the AUV should "head towards the wall", "keep heading straight" and "head away from the wall" is calculated. Following the previous example:

IF	AND	THEN	Membership	Equals
too far	getting closer	head towards	$\min(0.00,0.40)$	0.00
at desired	getting closer	head away	$\min(0.75,0.40)$	0.40
too close	getting closer	head away	$\min(0.25,0.40)$	0.25
too far	no change	head towards	$\min(0.00,0.60)$	0.00
at desired	no change	head straight	$\min(0.75,0.60)$	0.60
too close	no change	head away	$\min(0.25,0.60)$	0.25
too far	getting further	head towards	$\min(0.00,0.00)$	0.00
at desired	getting further	head towards	$\min(0.75,0.00)$	0.00
too close	getting further	head away	$\min(0.25,0.00)$	0.00

$$\begin{aligned} \text{head towards} &= \sqrt{0.00^2 + 0.00^2 + 0.00^2 + 0.00^2} \\ &= 0.00 \end{aligned}$$

$$\begin{aligned} \text{head straight} &= \sqrt{0.60^2} \\ &= 0.60 \end{aligned}$$

$$\begin{aligned} \text{head away} &= \sqrt{0.40^2 + 0.25^2 + 0.25^2 + 0.00^2} \\ &= 0.53 \end{aligned}$$

Finally, in the third process known as "Defuzzification", the centroid of the actions "head towards the wall", "keep heading straight" and "head away from the wall" is determined. For following a wall to the port (left) side of the AUV *Mako*, the value resulting from the Defuzzification process is used to adjust the starboard (right) motor such that the AUV performs the desired action. If the desired speed of the left and right motors is 50%, continuing the example, the speed adjustment for the right motor should be:

$$\begin{aligned} \text{output} &= \frac{-50(0.00) + 0(0.60) + 50(0.53)}{0.00 + 0.60 + 0.53} \\ &= 23.45\% \end{aligned}$$

That is, the AUV needs to slow down the right motor speed (or speed up the left motor speed) by 23.45% in order to head away from the wall.

To adjust or tune the Fuzzy controller, the x-intercepts of the member functions are moved. These values are what were used with the AUV *Mako* in this experiment. For more information about Fuzzy Logic, see [6].

5.2.4.4 Results

A video of wall following using Fuzzy Logic is available on the accompanying CD-ROM. The video shows the AUV *Mako* negotiating the pool steps.

The reliability of the Fuzzy Logic controller was witnessed to be far more robust than the proportional controller.

The plot below in Figure 39 shows wall following using Fuzzy Logic.

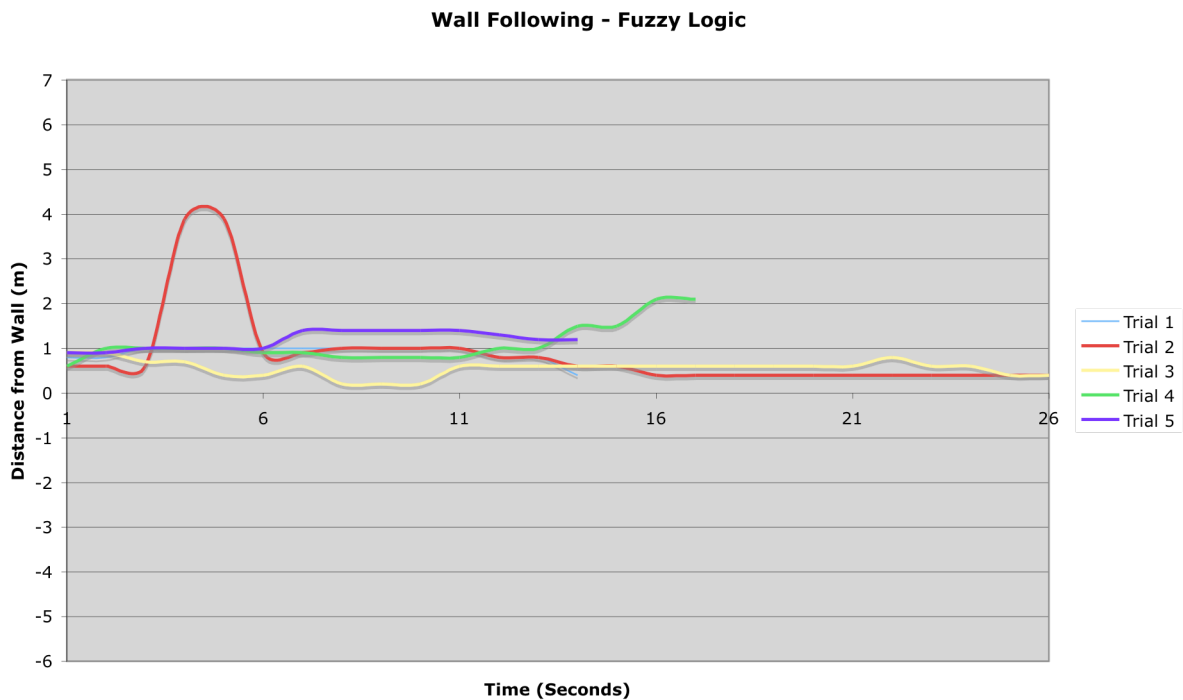


Figure 39: Wall following using Fuzzy Logic

5.2.4.5 Analysis

Unfortunately, the plot in Figure 39 does not accurately portray the robustness of the Fuzzy Logic controller compared to the proportional controller. Again the spikes in Trial 2 and Trial 4 are due to multipath interference at a change in angle of the pool wall. The Fuzzy Logic controller was observed during the experiment to be far better at maintaining the desired distance from the wall, and was better able to correct when initially placed at the wrong distance from the wall.

Chapter 6

Conclusion and Future Work

The design and testing of the new depth pressure sensor and sonar multiplexing system have been detailed in this thesis. The designs and theory presented in this thesis are not only relevant to UWA's AUV *Mako*, but also address problems faced by other AUV designers around the world.

6.1 Outcomes

This thesis project has achieved the following outcomes for the depth pressure sensor and the sonar multiplexing system.

6.1.1 Depth Pressure Sensor

A depth pressure for the AUV *Mako* has been successfully constructed and integrated during this project. The design was carefully considered and the result has been a depth pressure sensor with the linearity, stability and accuracy characteristics of an expensive commercial product. Arguably the depth sensor is the most important sensor on the AUV and as such, functionality and reliability were considered to be paramount.

The depth pressure sensor has been tried and tested in all of the pool experiments this year. Problems found relating to the sensor, such as the effects of the fluctuating supply voltage, have now all been addressed and the sensor should continue to operate as-is, without maintenance, for students in the coming years. Testament to the success of this sensor, the German-exchange Masters students are incorporating it into the sensor suit on UWA's new second AUV. Jonathan Brant from the Electronics Workshop has also expressed interest in using the amplifier design in future non-pressure sensor projects where possible.

6.1.2 Sonar Multiplexing System

This design aimed to enable the use of more sonar transducers on the AUV, without the use of any more serial ports. This aim has been achieved. The circuit, although

complex looking, provides a simple and extensible method of interfacing the two Navman Depth 2100 controllers and four transducers to *Mako's EyeBot*. It uses cheap and readily available components, and is easy to use through the C++ application program interface (API) developed to control it. With small modification, extra NMEA 0183-compatible devices can be added in the future, due to the modularity of the design.

Unfortunately the Navman Depth 2100 controllers, when used as a sonar system on the AUV, do have shortcomings that cannot be overcome. These include the slow sampling rate of 1Hz, which means that the AUV cannot travel at high speed if object detection is enabled, and the low resolution of 10cm.

6.2 Future Work

6.2.1 Depth Pressure Sensor

The depth pressure sensor is quite robust. However, if required, replacing the ABS plastic enclosure with a metal one would provide better electromagnetic interference performance. When selecting the enclosure, the metal enclosures available would have corroded in pool and seawater environments that the AUV is regularly used in. An aluminium or high-quality stainless steel enclosure is required, though none were readily available at the time of construction.

6.2.2 Sonar Multiplexing System

The sonar multiplexing system itself should work perfectly with no need for future modifications to improve performance. In the longer term, a better solution to the problem of accurate and fast sonar needs to be found. Nevertheless, this solution is effective for now. One possibly beneficial modification would be the introduction of attenuators in order to reduce the power output of the Navman Depth 2100 controller. This would hopefully reduce the multipath effects present in the shallow water pool environment.

6.3 Final Comment

Project Mako is now a final year project with a large capacity for expansion and future development. It represents a field of research that is at the forefront of

innovation at many universities around the world. With hard work, hopefully *Mako* can be the first Australian AUV to compete in the annual International Autonomous Underwater Vehicle Competition (IAUVC) in the coming years.

Appendix A

Depth Sensor API

The Depth Pressure Sensor C/C++ API, defined in `depth.h` and `depth.cc`, contains two functions.

```
int DEPTHReadRaw(void);
```

This first function returns the raw 10-bit ADC value (0-1023) value of the depth sensor. It samples the depth sensor analogue input three times. The middle value of the three samples is selected and returned.

```
int DEPTHRead(void);
```

This second function returns the depth of the lowest point on the AUV in millimetres, based on the calibration done in Depth Sensor Experiment 3. It uses the function `DEPTHReadRaw(•)` to obtain the middle value of three samples of the pressure sensor, then scales the result and returns it to the user.

Appendix C

Sonar Multiplexing System API

The Sonar Multiplexing System C++ API, defined in `sonar.h` and `sonar.cc`, contains four public functions inside the class `CSonar` along with a constructor and destructor.

```
int CSonar::Init(void);
```

This function initialises the `CSonar` object and the Sonar Multiplexing System. It must be called before anything else. Returns 1 on success.

```
int CSonar::ControllerPower(int controller1, int controller2);
```

This function turns on or off the power for the Navman Depth 2100 controllers. Can be used to save power if the AUV is low on batteries. The integers `controller1` and `controller2` can be 0 (power off), 1 (power on) or 2 (leave unchanged). Both controllers are powered up automatically inside `CSonar::Init(•)`. Returns 1 on success.

```
int CSonar::SelectTransducers(char controller1, char controller2);
```

Selects which transducers are to be connected to which controller. The character `controller1` can be 'f' (front), 'd' (down), 'n' (none) or null (leave unchanged). The character `controller2` can be 'l' (left), 'r' (right), 'n' (none) or null (leave unchanged). Returns 1 on success.

```
int CSonar::CurrentTransducers(char *controller1, char *controller2);
```

This function places the labels of the currently connected transducers (as in `CSonar::SelectTransducers(•)`) at the pointer locations `controller1` and `controller2`.

```
int CSonar::GetDistances(float *dist1, float *dist2);
```

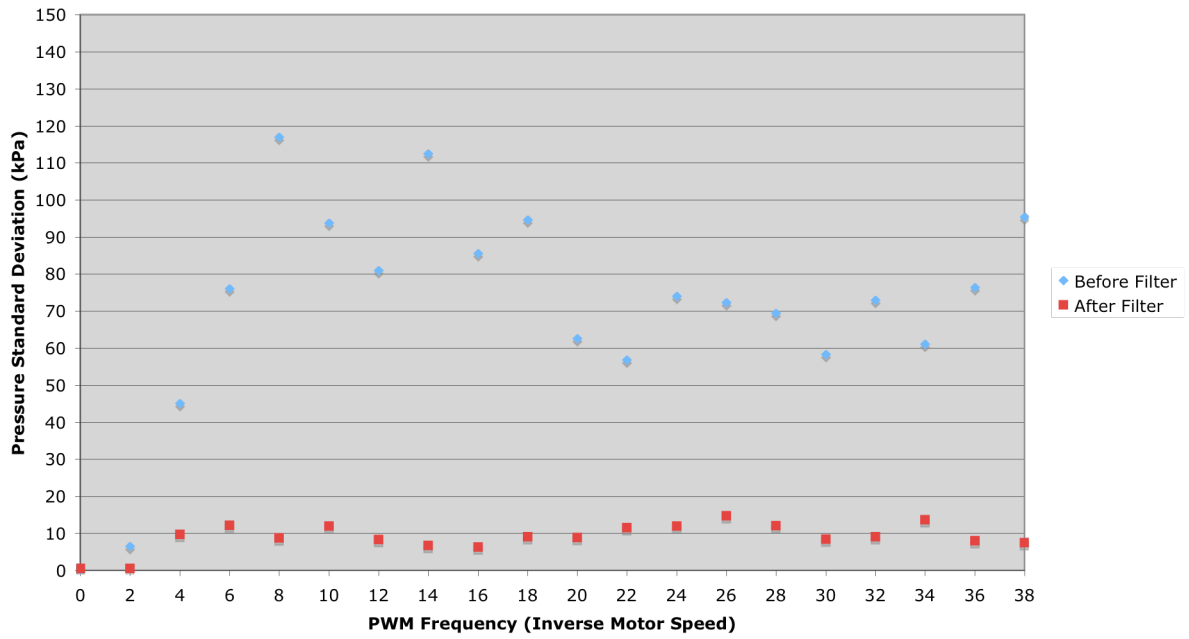
This function places the currently buffered values of the distances measured by Controller 1 and Controller 2, in metres, into locations `dist1` and `dist2`.

For an example on how to use the sonar multiplexing system API, please see the comments in `sonar.h`, located on the CD-ROM.

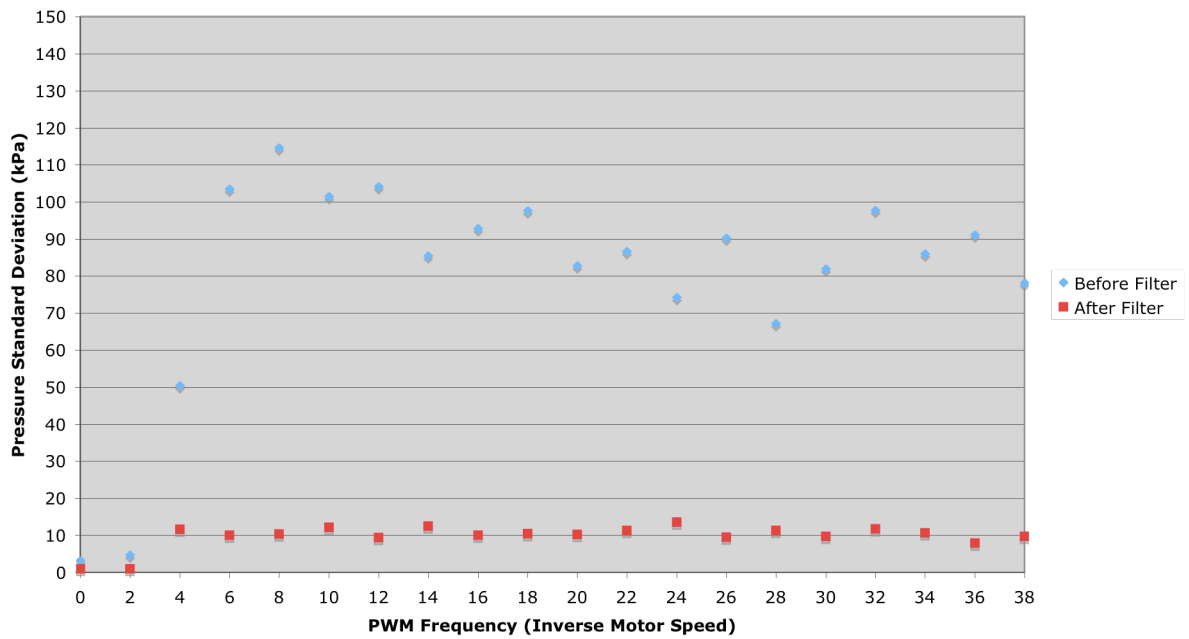
Appendix D

EMI Experiment Results - Continued

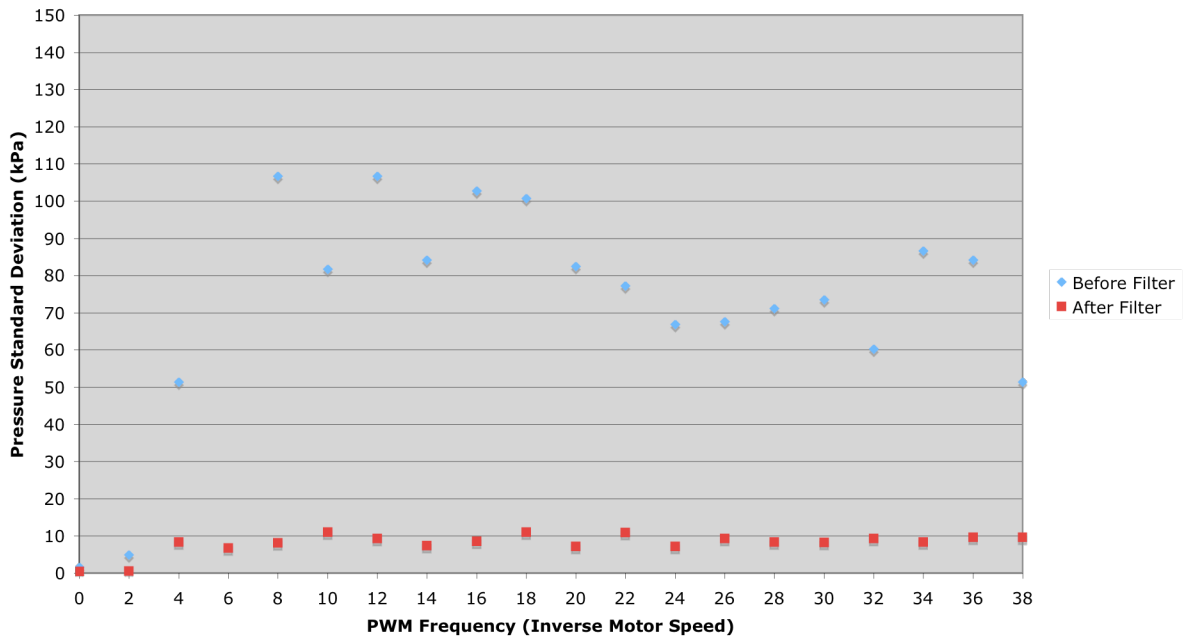
Port Motor - Forward Direction - Pressure Standard Deviation



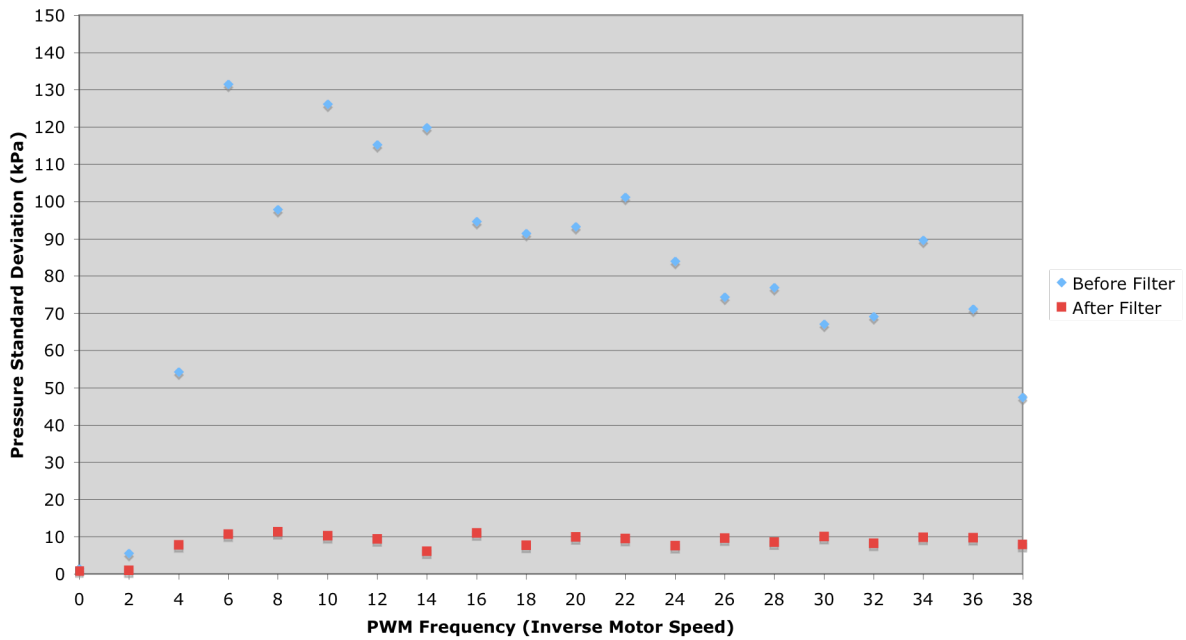
Port Motor - Reverse Direction - Pressure Standard Deviation



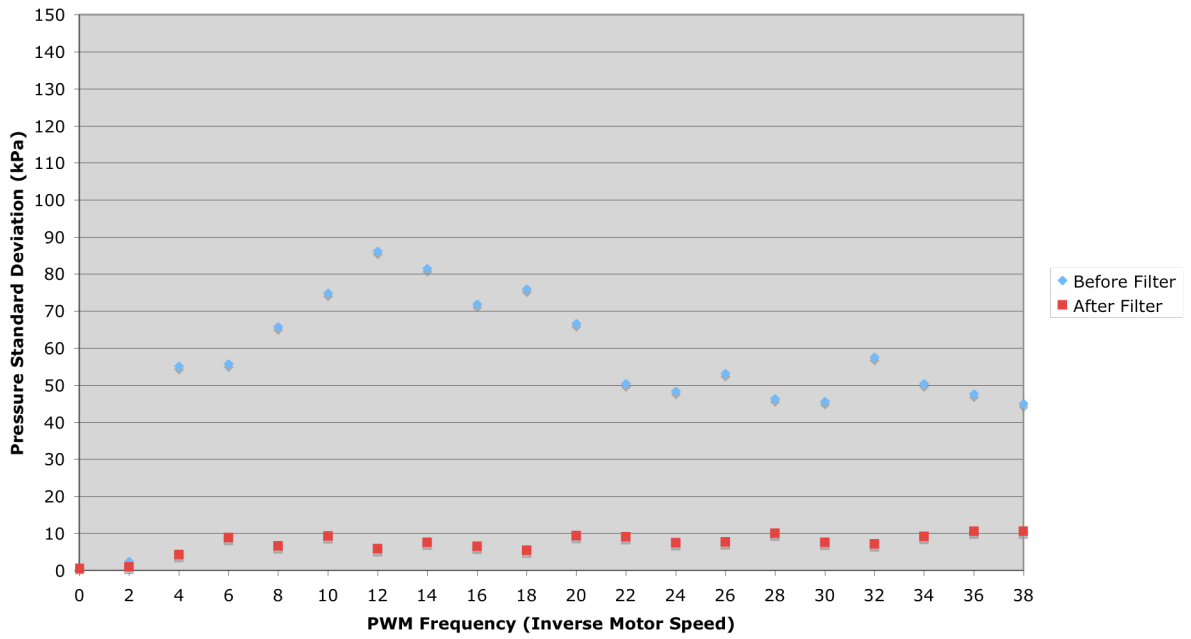
Starboard Motor - Forward Direction - Pressure Standard Deviation



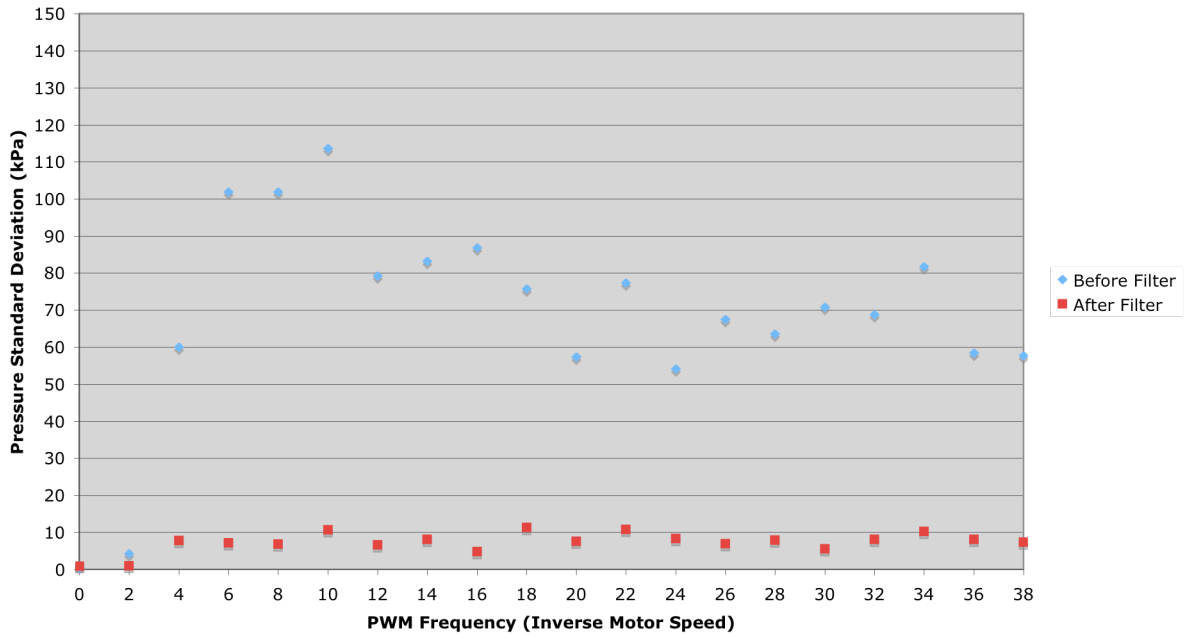
Starboard Motor - Reverse Direction - Pressure Standard Deviation



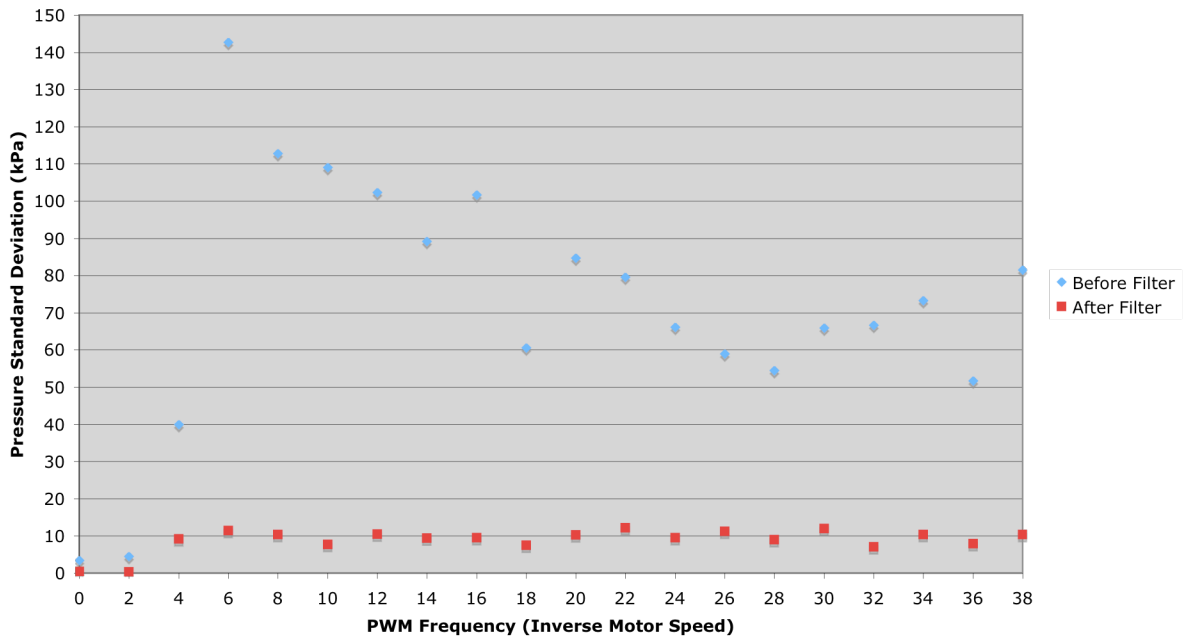
Bow Motor - Forward Direction - Pressure Standard Deviation



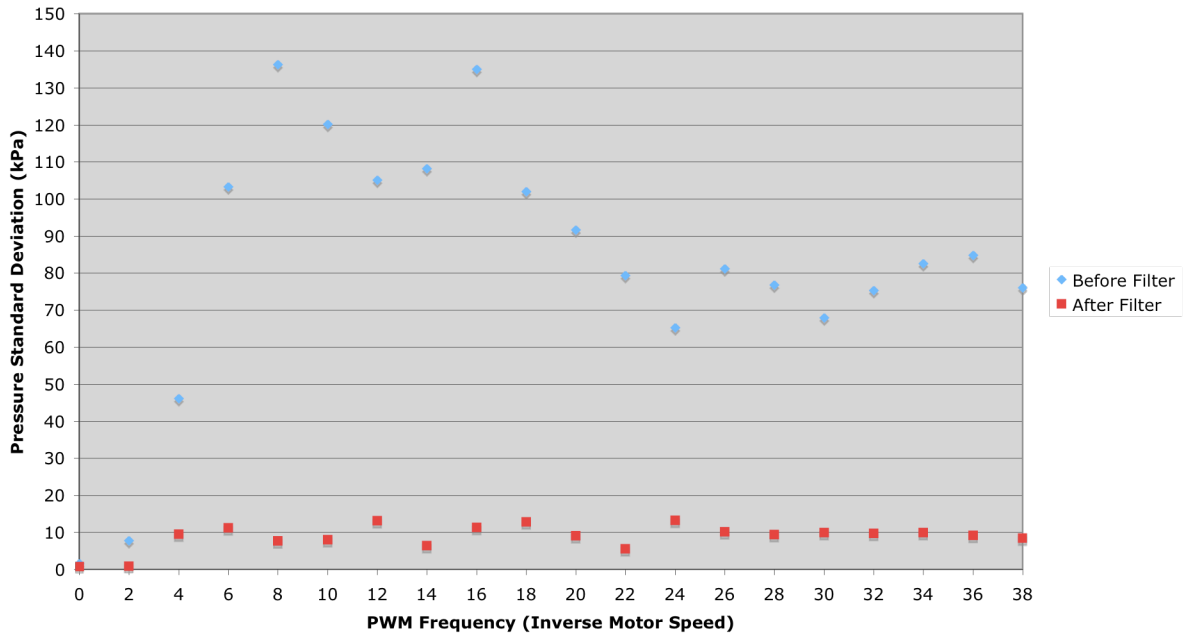
Bow Motor - Reverse Direction - Pressure Standard Deviation



Stern Motor - Forward Direction - Pressure Standard Deviation



Stern Motor - Reverse Direction - Pressure Standard Deviation

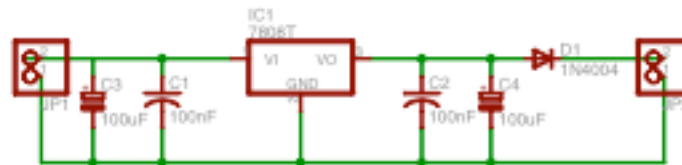


Appendix E

Voltage Regulator

The day before UWA Expo Day, the small 7.2V EyeBot voltage regulator board on the AUV began to fail. That night, a new regulator was designed and fabricated to ensure the AUV would work for the duration of Expo Day.

The design uses a 7808 (1-amp and 8-volt) voltage regulator integrated circuit (IC) in series with a 4-amp power diode to create a 7.2-volt regulated power supply. The schematic diagram of the new voltage regulator is shown below:



Elliot Alfirevich fabricated the new voltage regulator in the following steps:

1. The Printed Circuit Board (PCB) for the design was laid out manually in CadSoft EAGLE.
2. Utilising the fact that toner from a laser printer doesn't properly fuse to glossy inkjet paper, the final circuit board layout was printed onto Epson Glossy Inkjet Photo Paper.
3. With a very hot clothes iron, the toner and design was transferred cleanly off of the glossy photo paper and fused onto the blank PCB.
4. The blank PCB, now containing the design, was etched in a tank of bubble-agitated and heated Ammonium Persulphate.
5. The resulting circuit board was lacquered with spray-on varnish to prevent tarnishing of the copper traces.
6. The board was trimmed to size using a bandsaw.
7. The holes for components were drilled using a standard drill press with very fine tungsten-carbide drill bits.
8. The components were soldered in and the board tested.

Appendix F

CD-ROM Listing

Application Program Interface (API)

This directory contains the C++ source and header files for the depth pressure sensor and sonar multiplexing system application program interfaces (APIs).

It also contains example code demonstrating how to use each API.

Deliverables

This directory contains the Word documents and supporting files (images etc.) for this thesis document, the interim report and literature review.

Designs

This directory contains the designs for the depth pressure sensor, sonar multiplexing system and voltage regulator. Included in this directory are the schematics, PCB layouts, photographs and relevant PICAXE source code for each project, where available.

Experiments

This directory contains the results, EyeBot software and photographs for each of the experiments detailed in this thesis.

Media

This directory contains:

- the Expo Day photographs;
- the Expo Day poster designs;
- the AUV stickers and badge designs;
- the t-shirt designs; and,
- videos from various pool tests.

Presentations

This directory contains the PowerPoint presentations and supporting files (image etc.) for the Five-Minute Presentation, Fifteen-Minute Presentation and Final Presentation.

Bibliography

- [1] J. Ablitt, *Speed of Sound in Seawater*, U.K. National Physics Laboratory, [online], August 2001. Available:
<http://www.npl.co.uk/acoustics/techguides/soundseawater/content.html>

- [2] R. Altshuler, *ORCA-VII: An Autonomous Underwater Vehicle*, [online], 2004. Available:
<http://web.mit.edu/orca/www/2004Materials/MITJournalPaper2004.pdf>

- [3] AUVSI. Association for unmanned vehicle systems international, [online], 2004. Available: <http://www.auvsi.org/>

- [4] G. Beecham, *Boyle's Law*, wikipedia.org [online], December 2004. Available:
http://en.wikipedia.org/wiki/Boyles_law

- [5] P. Bennett, *The NMEA FAQ*, [online], 12 June 2003. Available:
<http://vancouver-webpages.com/peter/nmeafaq.txt>

- [6] T. Bräunl, *Fault Tolerant Computer Systems 422*, "5. Fuzzy Logic". School of Electrical, Electronic and Computer Engineering, University of Western Australia, 2005.

- [7] J. Chiappa, *Fluid Pressure*, wikipedia.org [online], December 2004. Available:
http://en.wikipedia.org/wiki/Fluid_pressure

- [8] Cornell University's Autonomous Underwater Vehicle (CUAUV), [online], 2003. Available: <http://www.cuauv.org/>

- [9] Diving Science & Technology, *PADI Open Water Diver Manual*. California: International PADI, Inc., 2003

- [10] Duke Robotics, *AUV Overview: Pressure Sensor* [online], October 2005. Available:

http://www.duke.edu/web/robotics/html/auv_electrical_overview_pressure_sensor.htm

- [11] Global Water Datasheets, *WL400 Fluid Level Transducer*, [online], 2004. Available: <http://www.globalw.com/downloads/WL400/WL400manual.pdf>
- [12] GlobalSecurity.org, *Tethered Unmanned Work Vehicle System (Super Scorpio ROV)*, [online], August 2005. Available: <http://www.globalsecurity.org/intell/systems/tuwvs.htm>
- [13] L. Gonzalez, *Design, modelling and control of an autonomous underwater vehicle*. Honours thesis. School of Electrical, Electronic and Computer Engineering, The University of Western Australia, WA, Australia, 2004.
- [14] HowStuffWorks, *How Submarines Work*, [online], 2003. Available: <http://science.howstuffworks.com/submarine1.htm>
- [15] Motorola Semiconductor Technical Datasheets, *MPX5100 Series*, [online], October 2005. Available: <http://www.atmicroprog.com/download/autres/mpx5100.pdf>
- [16] Nautronix P.L.C, *NASNet™: Nautronix Acoustic Subsea Network*, [online], October 2005. Available: <http://www.nautronix.com/web/articles/product.asp?id=1071>
- [17] Navman Pty. Ltd., "Install and Operation Manual", Navman Pty. Ltd., [manual]
- [18] M. Nguyen, *Design of an active acoustic sonar sensor system for an autonomous underwater vehicle*. Honours thesis, The University of Western Australia, 2004.
- [19] Rama, *Sonar*, wikipedia.org [online], March 2005. Available: <http://en.wikipedia.org/wiki/Sonar>

-
- [20] Revolution Education, *PICAXE Datasheets*, [online], October 2005. Available: <http://www.rev-ed.co.uk/picaxe/data.asp?mode=all>
- [21] D. Sampson, *Optical & Wireless Communication Part 2*, "Lecture 19: Radar". School of Electrical, Electronic and Computer Engineering, University of Western Australia, 2005.
- [22] Samson AG, *Serial Data Communication*, [online], October 2005. Available: http://www.samson.de/pdf_en/l153en.pdf
- [23] Science of Sound in the Sea, *How fast does sound travel?*, [online], October 2005. Available: <http://www.dosits.org/science/sndmoves/1.htm>
- [24] Sea-bird Electronics, Inc., *SBE 50 Datasheet*, [online], September 2003. Available: http://www.seabird.com/pdf_documents/datasheets/50brochureSept03.pdf
- [25] Sensotec Datasheets, *Pressure Transducers: Model TJE*, [online], 2005. Available: <http://www.sensotec.com/pdf/tje.pdf>
- [26] SenSym Application Department, *IC Sensor Signal Conditioning SSAN-16*, "Programmable Current Source Provides Novel Method of Span Compensation," [online], February 1998. Available: <http://sensor.com.tw/sensym/application/ssan16.pdf>
- [27] SenSym Datasheets, *SX Series Sensors*, Farnell, [online], 2004. Available: <http://www.farnell.com/datasheets/51886.pdf>
- [28] The PAST Foundation, *The Development of ROV Technology*, [online], 2004. Available: <http://www.pastfoundation.org/DeepWrecks/ROVTechnology.htm>

-
- [29] C. Thorp, *Control System for an Autonomous Underwater Vehicle*, Honours thesis. School of Electrical, Electronic and Computer Engineering, The University of Western Australia, WA, Australia, 2005.
- [30] United States Naval Academy, *USNA 2002 AUV Depth Sensor*, [online], 2002. Available: http://www.usna.edu/AUVT/subsystem_depthsensor.htm
- [31] U.S. Department of State's Bureau of International Information Programs, *U.S. Rushing To Save Russian Sailors Trapped on Sunken Submarine*, [online], August 2005. Available: <http://usinfo.state.gov/eur/Archive/2005/Aug/05-410751.html>